



**Mobile Robots with Novel Environmental Sensors  
for Inspection of Disaster Sites with Low Visibility**

Project start: January 1, 2015

Duration: 3.5 years

## **Deliverable 5.1**

### **Algorithms for Sensor Planning**

Due date: month 36 (January 2018)

Lead beneficiary: ORU

**Dissemination Level: Public**

**Main Authors:**

Victor Hernandez Bennetts (ORU)

Asif Arain (ORU)

Erik Schaffernicht (ORU)

Achim Lilienthal (ORU)

**Version History:**

0.1: initial version, VH, May, 2018

## Contents

Contents.....	3
A    Introduction and purpose of this document .....	4
B    Sensor Planning for In-situ gas sensors.....	4
B.1    Model-free sensor planning approach .....	5
B.2    Model-based sensor planning approach .....	7
C    Sensor Planning for remote sensors .....	9
C.1    Adaptive sensor planning for remote sensor .....	10
D    Sensor planning for communication coverage .....	12
E    Summary and Outlook.....	14
References .....	15
Appendices.....	16

## A Introduction and purpose of this document

In this deliverable, algorithms are proposed to efficiently conduct an exploration mission to cover the target area as fast as possible while acquiring relevant information. For example, the robot prototype should identify interesting areas where emitting gas source locations might be located. In the Smokebot scenario, the exploration strategy (robot trajectory and stop positions) is decided by the human operator. Thus, the planning algorithms presented in this deliverable should be able to suggest positions of interest (POI). These POIs are places where the multiple sensor readings will be most informative to integrate into the GDIM, will help localizing a gas source or where dropping a wireless repeater will ensure stable communication with the operator. Two different types of problems are considered: coverage - building an environment model of the whole operation area as quickly as possible - and exploitation - observing a specified small area for detailed information gathering over time.

The POIs are presented to the human operator, which then decides where to move the robot based on the priority that each of the tasks has at a given point in a guven mission. For example, the operator might decide to prioritize POIs related to gas sensing, and move the robot accordingly, if localizing gas leaks is a priority during the mission.

In the following sections, the different sensor planning algorithms developed in Smokebot, are presented. Based on the sensors' characteristics, the algorithms are grouped as follows:

- a) **Sensor planning for in-situ gas sensors (Section B):** For example, suggesting interesting positions to localize emitting gas sources.
- b) **Sensor planning for remote sensors (Section C):** For example, suggesting possitions for LIDAR sensors to minimize thermal reflection.
- c) **Sensor planning for communication coverage (Section D):** For example, predicting areas with low RF signal coverage ahead of the robot.

## B Sensor Planning for In-situ gas sensors

In-situ gas sensors are devices that require direct contact with the analyte under study in order to report a measurement. This means that the reported measurement corresponds to only a few centimeters around the location of the sensor, which makes data acquisition time consuming. In order to efficiently conduct an exploration mission under autonomy limitations, such as in the case of Smokebot, a sensor planning strategy is required. We developed two different sensor planning strategies for in-situ gas sensors for the task of gas source localization. The first strategy is a model-free, data driven approach that creates a lattice where at each cell, an estimation of the distance to a gas source is stored. Areas that are predicted as being nearby the source can be considered as POI. The distance estimations at those cells not visited by the robot are computed using Gaussian regression guided by wind flow measurements. The second approach is model based. Specifically, it uses Partial Differential Equations for gas source localization. Construction a realistic mathematical model of gas dispersion is complex and computationally expensive to solve. To address this problem, we propose a probabilistic model based on diffusion PDE to approximate the complexities of gas dispersion. The model suggest informative measurement locations as well as likely source locations. The proposed approaches were evaluated in real-world and with hardware-in-the-loop experiments respectively. The following sections present a deeper overview of the algorithms and the results achieved in the experimental validation processes.

## B.1 Model-free sensor planning approach

This algorithm represents the target environment  $M$  as a lattice of cells of identical size:  $M=\{x_1, \dots, x_N\}$ . The algorithm assumes that only one gas source is present in the environment. Regarding on-board sensing modalities, the algorithm assumes that the robot is equipped with gas and airflow sensors and moreover, it assumes that the robot's position is available.

The robot moves between the centers of the cells. After each movement it records measurements of gas concentration and wind information for a certain amount of time in order to compute the source distance estimation. We define a function  $f(x)$  that is unknown a-priori and is updated from noisy observations.  $f(x)$  indicates the distance to the source at location. Using measurements at visited locations, the robot extrapolates  $f(x)$  to estimate non visited locations. The algorithm uses these estimations to decide where to measure next in order to improve the model efficiently. The overall process is computed online as the robot traverses the target area.

Fig. 1(a) shows the three functional blocks of our proposed model-free algorithm. In the first block, an estimation of the distance to the gas source is computed. We use the method proposed by Schmuken and co-authors in [1], which correlates the variability of the sensor response to the distance to the source. A key element to the algorithm proposed by the authors is the detection of bouts in the sensor response. These bouts correspond to the rising edges of the sensor signal, as shown in the example in Fig. 1(b). In [1], it is reported that there is a strong correlation between the number of bouts and the distance to the gas source: the higher the bout count, the closer the sensor to the gas source. To detect the bouts, a cascaded filtering approach is used to detect fast transients in the sensor signal. A low-pass filter is first used in order to remove high-frequency noise.

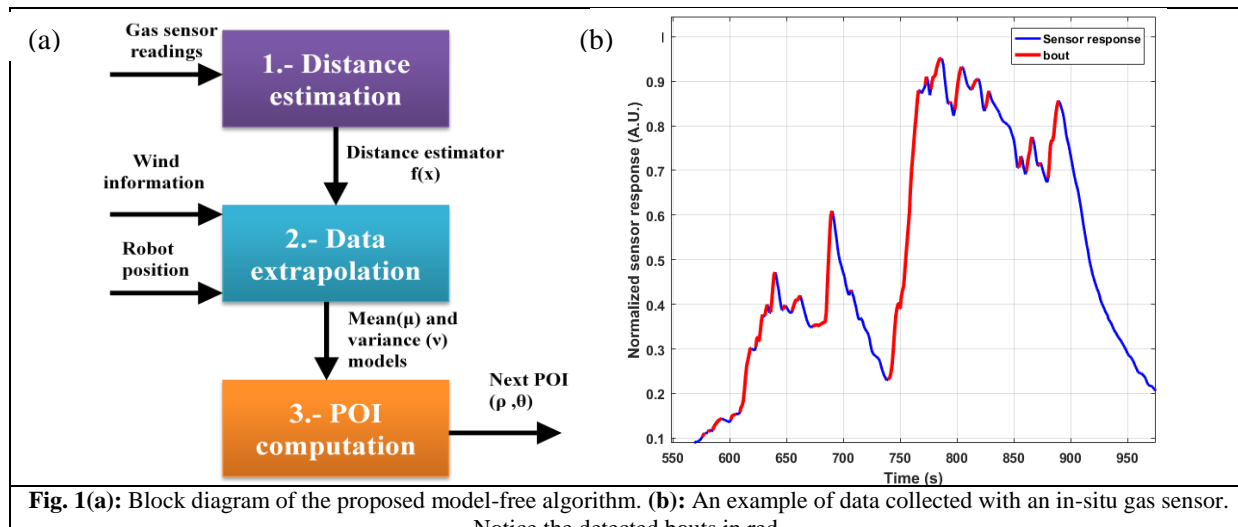


**Fig. 1(a):** Block diagram of the proposed model-free algorithm. **(b):** An example of data collected with an in-situ gas sensor. Notice the detected bouts in red.

To evaluate the applicability of the bout approach, we used an array of six commercial MOX sensors<sup>1</sup> on-board a mobile robot to collect data at different locations of an indoor corridor where a gas source is located. The gas source is a plastic container filled with ethanol. A bubbler facilitates evaporation while a fan placed nearby the source allows to spread the analytes away. As shown in Figure 2(a), no correlation between bout count and distance to the source is observed. This is in stark contrast with what is stated in [1]. The reason for this is that the authors conducted their experiments inside a wind tunnel with controlled airflow conditions. We proposed a novel indicator of source proximity using the bout approach. Instead of counting bout occurrences, we calculate the bout amplitudes. As can be seen

<sup>1</sup> <https://www.sgxsensorstech.com/>

in Fig 2(b), the average bout amplitude is a good indicator of the distance to the gas source in uncontrolled environments. In some cases, when moving away from the source by 0.5 m the average amplitude slightly increases. However, in most cases, the average bout amplitude decreases when moving away from the source for more than 1 m.

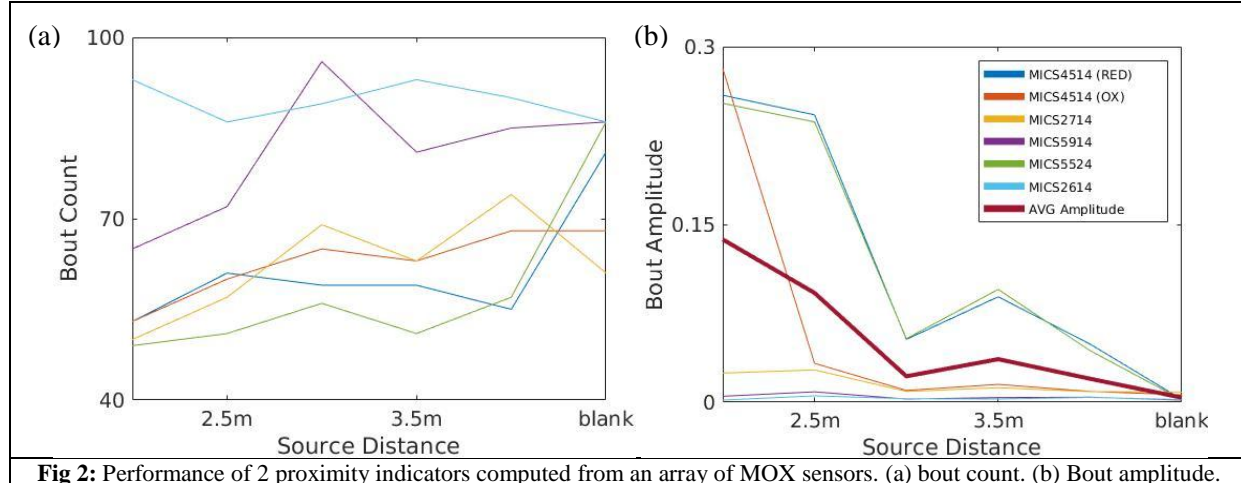


**Fig 2:** Performance of 2 proximity indicators computed from an array of MOX sensors. (a) bout count. (b) Bout amplitude.

The next step in the algorithm is the estimation of  $f(x)$  at non visited locations (Fig 1(a)). We thus model the average bout amplitude  $\mu$  as a Gaussian process with a radial kernel function, stretched according to the wind direction as proposed in [2]. One of the advantages of using Gaussian regression process is that it estimates the a-posteriori variance  $v$ . The kernel corresponds to the assumption that positions in upwind direction have bout amplitudes similar to the measurement point. It also expresses the exploitation component of the exploration strategy, which leads the robot to follow a gas plume. Fig. 3(a) show examples the effect of the wind vector over the kernel while Fig. 3(b) shows the result of the extrapolation method from data collected with the robot.

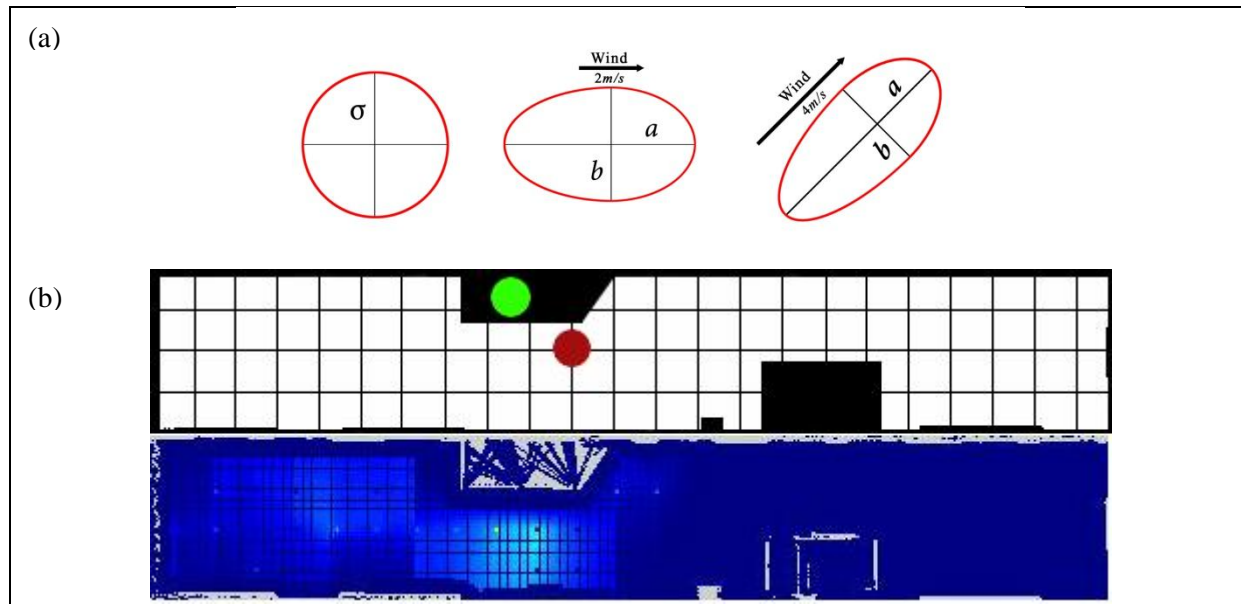


**Fig. 3:** (a) Influence of the wind speed and direction on the shape of the kernel. The ellipse is rotated according to the wind direction. The semimajor axis  $a$  is stretched in the upwind direction and shrunk in the downwind direction according to the wind speed. (b) An example of a bout amplitude map. In the upper plot (i.e. the grid map), the green circle indicates the gas source and the red circle the final position of the robot. The bottom plot corresponds to the mean bout estimate. The dark blue regions map areas with low bout amplitude estimates, whereas the light blue indicates high mean values.

To suggest Point Of Interest (POI) to the operator (Step 3 in figure 1(a)), a trade-off between exploration of unvisited areas (following the variance gradient) and exploitation (following the direction to the highest bout amplitude estimate). The next POI corresponds to a movement of  $\rho$  meters from the current position with a direction of  $\theta$ . The next POI will either be a position closer to the location with the highest variance (exploration) or a position closer to the highest bout amplitude estimate.

To test our proposed approach, we ran 12 experiments in the indoor scenario previously described. We consider an experiment successful if the robot chooses as the final position the reachable cell nearest to where the gas source is placed. A total of 8 runs were deemed successful, giving our method a 67% success rate. Reasons that could explain the failed experiments include the high wind speeds (which lead to bouts that cannot be resolved) and that the plane in which the robot sampled gas concentrations was at a substantially lower height than the gas source.

## B.2 Model-based sensor planning approach

In Smokebot, we also developed a model-based approach for sensor planning. We used a gas dispersion model based on Partial Differential Equations (PDE), in order to address gas distribution mapping and gas source localization. To address concerns related to computational cost, we propose a probabilistic model based on diffusion PDE to approximate the complex behavior of gas dispersion. Such model allows to identify likely locations of gas sources and to suggest POI to human operators.

Physical mechanisms causing gas propagation are not trivial, and in case of turbulence can even exhibit non-deterministic and chaotic behavior [3]. Nonetheless, for on-line mapping scenarios a simplified approximation of the physical phenomenon with low computational complexity might be of great use. To this end, we investigated the capability of a diffusion partial differential equation (PDE) to approximate spatial gas dynamics for the purpose of identifying sources that drive the gas propagation.

Regarding sensor planning, we build upon known methods that use, for example, linear-quadratic control techniques [4], optimal experimental design and probabilistic approaches [5]. We then propose an exploration strategy that minimizes the uncertainty of the source localization following a criterion similar to an A-optimality [6]. Additionally, similar to [7] we exploit the assumption that the sources causing gas dispersion are sparsely distributed and use sparse Bayesian learning techniques to model this.

From a practical perspective, approximating complex gas dynamics with simple models can be of an advantage. In Smokobot, we use a 2D diffusion model that can be formally described with a linear parabolic partial differential equation (PDE) that creates a spatio-temporal model of the gas concentration as follows:

C.1	$\frac{\partial f(\mathbf{x}, t)}{\partial t} - \kappa \Delta f(\mathbf{x}, t) = u(\mathbf{x}, t)$
-----	--

In the above equation,  $\mathbf{x}$  corresponds to a 2-D position,  $t$  corresponds to time and  $\kappa$  corresponds to a diffusion coefficient. The term  $u(\mathbf{x}, t)$  on the right hand side represents a spatio-temporal inflow of material; in this work we aim to identify this process.

In order to solve a PDE, numerical approximation methods are often the instrument of choice. To this end we begin with a classical Finite Difference Method [8] which “transforms” our diffusion PDE into

a finite dimensional linear system by appropriately discretizing both space and time. In other words, we divide our region of interest into a finite number of grid cells and consider temporal evolution of concentration values in each cell at discrete time steps n.

To facilitate numerical estimation of the PDE, we assume that gas dispersion mechanisms are complex and not always deterministic and that gas concentrations are not observed directly, but are rather measured with a sensor. This permits us taking a probabilistic approach toward PDE solution by treating all variables as random. We also assume that the gas sources are sparse in space, i.e., the gas distribution is only driven by a few unknown discrete sources, which allows us to use Sparse Bayesian Learning (SBL) techniques [9, 10]. Using Bayes theorem, the overall problem is reduced to estimating the PDFs of variables such gas concentrations at the cells in the grid, the location of the gas sources. The derivation of the equations of our algorithm can be consulted in Appendix II and III.

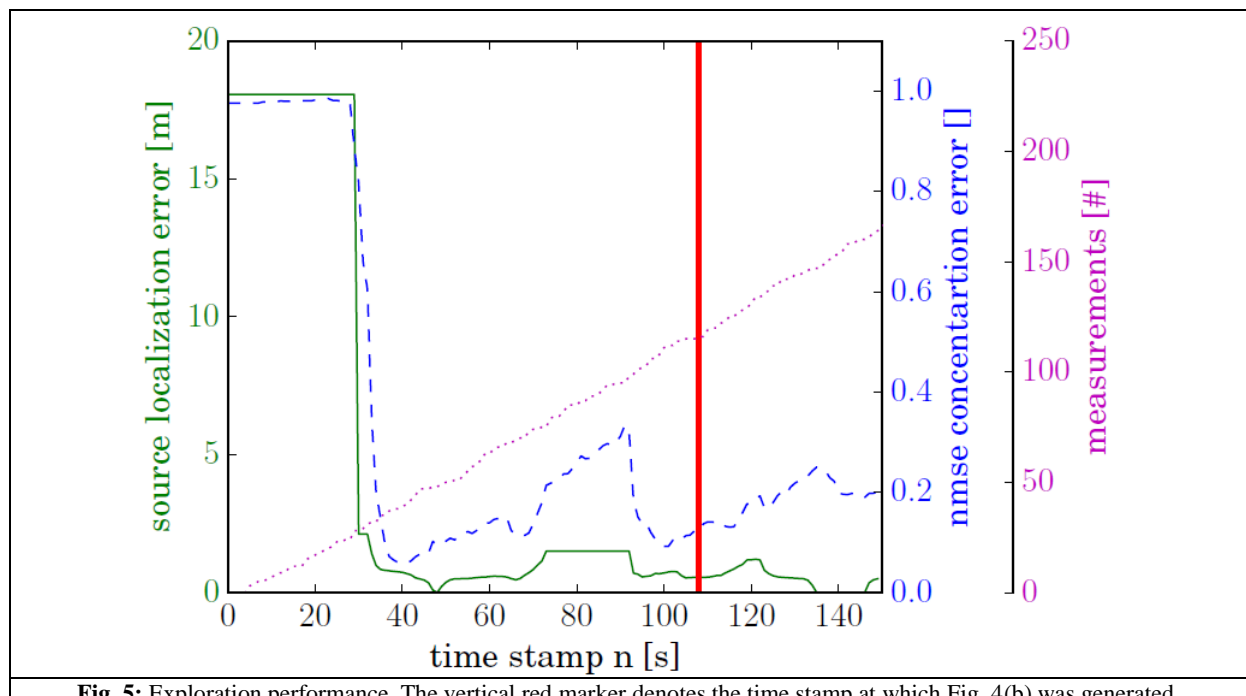
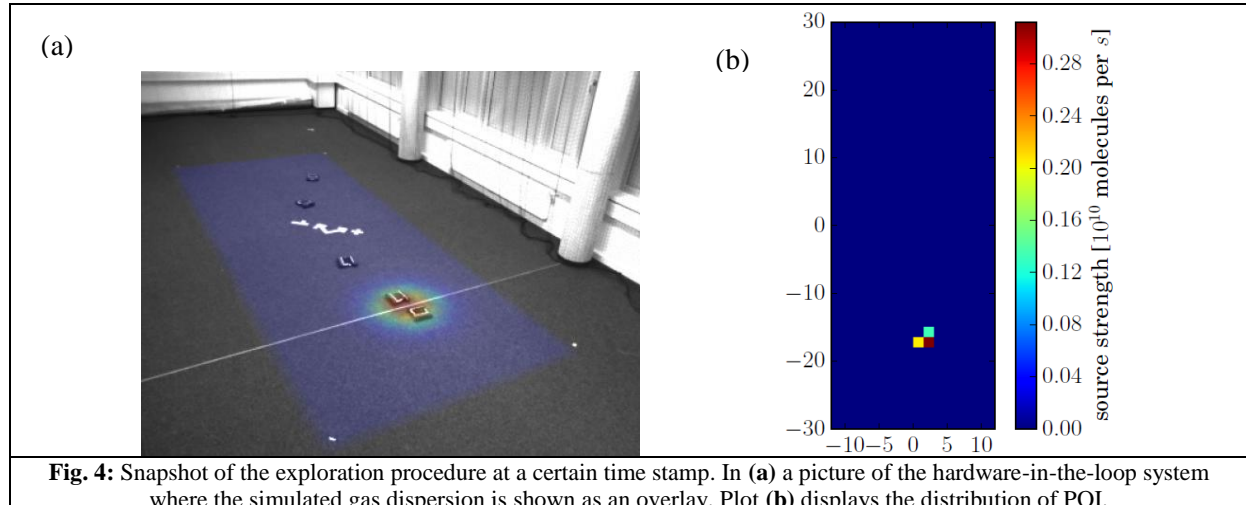
With what respect to sensor planning and the identification of POI, we take advantage of our probabilist framework. Specifically we consider that a high variance of the estimated gas source marginal PDFs implies a high uncertainty. This quantity can be used to rate all cells in the region of interest, and cells with highest uncertainties can be provided to the human operator as proposals for new measurement locations.

With what respect to sensor planning and the identification of POI, we take advantage of our probabilistic framework. Specifically we consider that a high variance of the estimated gas source marginal PDFs implies a high uncertainty. This quantity can be used to rate all cells in the region of interest, and cells with highest uncertainties can be provided to the human operator as proposals for new measurement locations.

In addition, we implemented an automatic exploration strategy that can be used for one or several autonomous platform. In our approach, the robot(s) selects a cell based on the uncertainty value and additionally weighted by the distance to it. In other words, the robots not only prefer cells with high uncertainty but also cells which are close to their current positions. When a target is reached, a measurement is taken, which maximally reduces the uncertainty of the corresponding grid cells.

For evaluation purposes, we used a hardware-on-the loop approach where gas dispersion was generated using a state-of-the-art simulator. We generated a dynamic gas distribution driven by one source in an area of 20m times 60m. In this environment, we used our proposed approach and a small number of robots. Whenever a robot is triggered to collect a measurement, the simulated gas concentration at the robots position is used as a synthetic measurement for the exploration algorithm.

Fig. 4 visualizes the result of the exploration at a certain time step, whereas Fig. 5 depicts the performance of the estimates over time. The source localization error is calculated by comparing the center of mass of the estimated source distribution with the actual position of the source used in the simulation. The concentration estimate is assessed by the Normalized Mean Square Error (NMSE) with respect to the concentration given by the simulator. Although the difference between the simulated gas concentration and the estimated concentration based on the simplified model is rather high due to the over simplifying diffusion approximation, the estimated source strength distribution is quite accurate and the robots are able to localize the source in a reasonable time frame with good accuracy.



### C Sensor Planning for remote sensors

Remote sensors acquire information or measurements without direct contact with the object under study. Examples of remote sensors are LIDARs, cameras and gas sensors based on spectroscopy principles such as TDLAS (Tunable Diode Laser Absorption Spectroscopy). In Smokebot, we developed an adaptive sensor planning algorithm that considers two key parameters in remote sensing, namely field of view and the range of the sensor. By field of view we refer to the extent of the observable world that is sensed at a given time. We define field of view by an angle through which the device is sensitive.

We test our proposed algorithm by addressing the task of gas sensing using a remote sensor. In our gas sensing task, we consider coverage of the area of interest and the estimation of a gas distribution map that includes sensing coverage to detect gas leaks and building a gas distribution model to

accurately locate the gas concentrations in the environment. As a sensing device, we use a Tunable Diode Laser Absorption Spectroscopy (TDLAS), which can collect integral concentrations along the line-of-sight. By mounting the TDLAS on a pan-tilt unit, optical beams can be projected in different direction and therefore, circular sector of range  $r$ , whit a field of view  $\phi$  can be sampled.

When such actuated TDLAS is mounted on a mobile robot (Fig. 6), data can be acquired at different poses  $(x,y,\theta)$ , which we refer to as a sensing configuration  $c$ . Thus, a solution for the surveillance task is a tour composed of a number of sensing configurations  $\{c_1, c_2, \dots, c_n\}$ . An efficient plan has a limited number of sensing configurations and a short traveling distance while at the same time, it provides a high sensing coverage with an accurate gas distribution model.

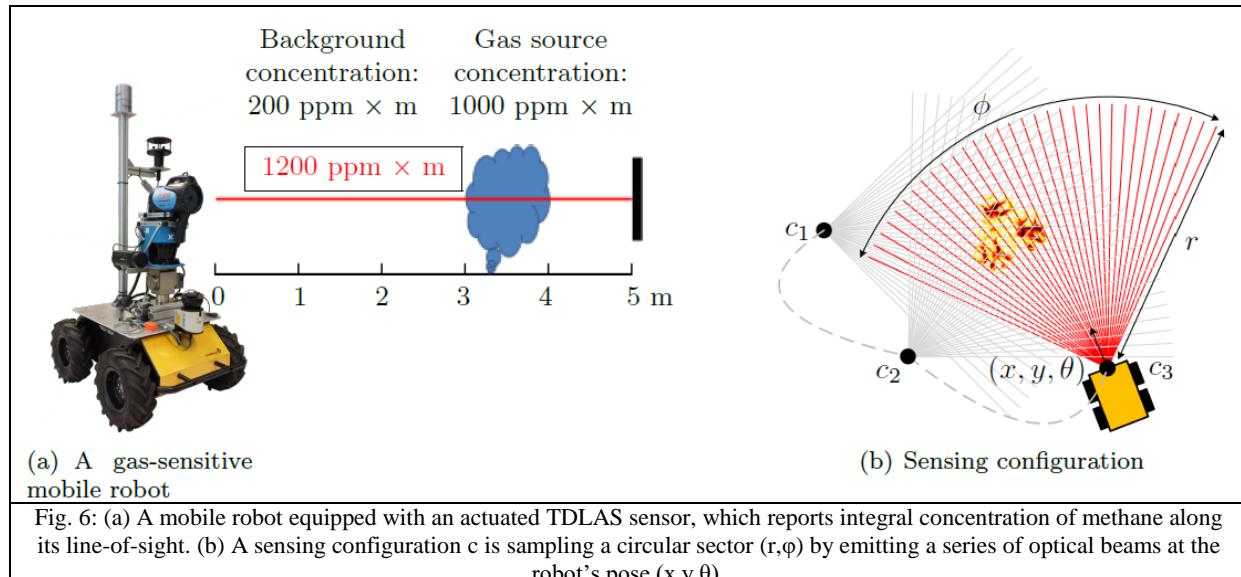


Fig. 6: (a) A mobile robot equipped with an actuated TDLAS sensor, which reports integral concentration of methane along its line-of-sight. (b) A sensing configuration  $c$  is sampling a circular sector  $(r, \phi)$  by emitting a series of optical beams at the robot's pose  $(x, y, \theta)$ .

## C.1 Adaptive sensor planning for remote sensor

As previously stated, Smokebot considers coverage and exploitation as key problems in sensor planning. In the context of remote gas sensing, coverage refers to scanning the whole target environment in order to identify areas of high concentrations. Exploitation refers to gathering detailed information in “areas of interest” in order to estimate the gas distribution map.

In our proposed algorithm, we conduct exploration and exploitation in a single measurement tour. Initially, a set of sensing configurations that guarantee the full exploration of the area under surveillance are estimated (as originally presented in [11]). Then, when an interest location is identified (i.e. an area that shows high gas concentrations), exploitation is conducted by suggesting sensing configurations that maximize the accuracy of the gas distribution map.

We represent the environment in a Cartesian grid of occupied and free cells. In addition, we consider a discrete number of candidate sensing configurations; this means that we consider only the locations at the centre of each cell and a limited number of orientations (e.g.  $0^\circ$ ,  $90^\circ$ ,

$180^\circ$ ,  $270^\circ$ ). The coverage is the capture by a matrix  $V$  of size equal to the number of candidate configurations times the number of free cells  $S$ .

A sensor planning solution for exploration is referred to as  $\pi_{\text{detect}}$ , which is a list of sensing configurations that provides the desired sensing coverage.  $\pi_{\text{detect}}$  is estimated by solving the optimization problem in Equation C.1, where  $C$  is a binary decision vector of candidate sensing configurations, and  $C$  is the sensing coverage provided by the selected configuration. The parameter  $n_{\text{cov}}$  determines the required coverage percentage.

C.1

$$\pi_{\text{detect}} = \operatorname{argmin} |C| \text{ s.t. } C \geq n_{\text{cov}}$$

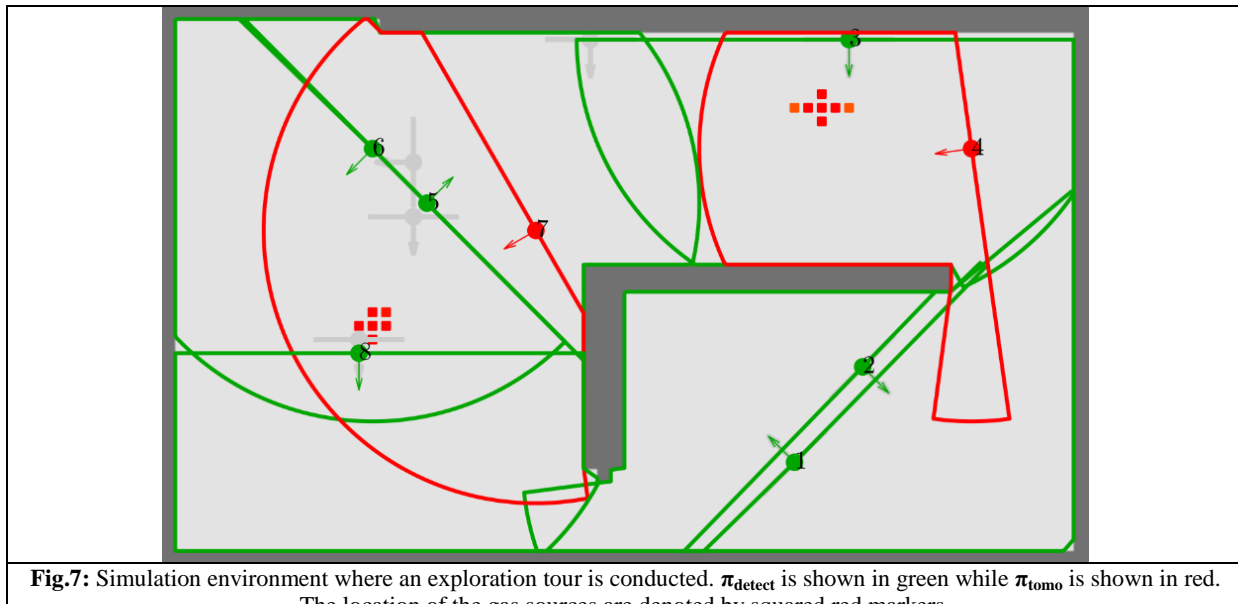
For the exploitation problem, we estimate  $\pi_{\text{tomo}}$ , which aims to provide an accurate gas distribution map. The accuracy of the gas distribution map is measured by  $Q$ , which is an arbitrary quantity inversely proportional to the error between the estimated and the true gas distribution. In a systematic evaluation (presented in [12]) we concluded that sensing configurations that have overlapping fields of view provide a better estimation of the gas distribution and thus a higher  $Q$ . As  $\pi_{\text{detect}}$  is being executed, areas of interest are identified, which then need to be sampled from different view points and sensing overlaps [12]. Equation C.2 is the optimization problem for exploitation, where  $n_{\text{tomo}}$  is the desired reconstruction quality and  $Q$ .

C.2

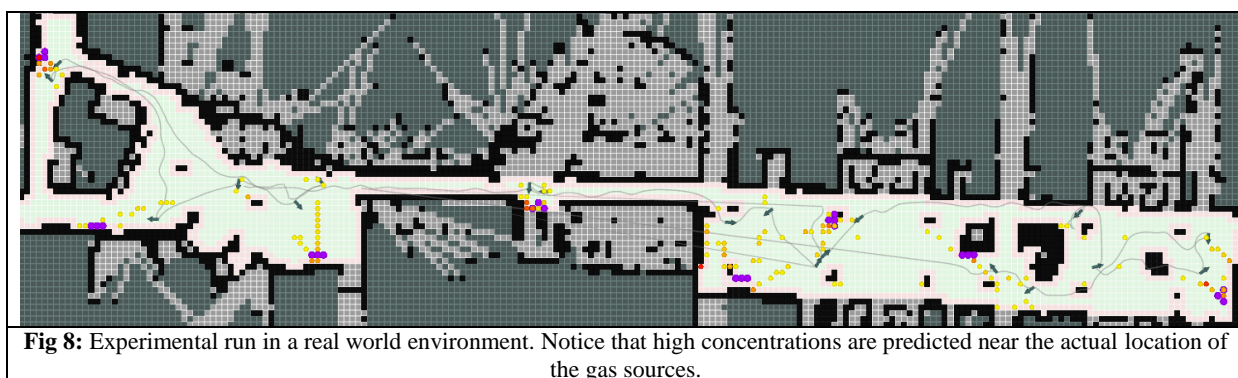
$$\pi_{\text{tomo}} = \operatorname{argmin} |C| \text{ s.t. } Q \geq n_{\text{tomo}}$$

Given the above solutions for the exploration and exploitation, our sensor planning algorithm can be summarized as follows: First, we estimate  $\pi_{\text{detect}}$  and we start executing it by collecting measurements at the suggested locations. If a high gas concentration is detected, then  $\pi_{\text{tomo}}$  is computed for all the neighbouring high concentration areas. The plan  $\pi_{\text{tomo}}$  is iteratively executed and improved for each selected configuration. At the end of an exploitation process,  $\pi_{\text{detect}}$  is re-computed for the remaining unexplored areas. This process continues until no configuration is left in  $\pi_{\text{detect}}$ .

To illustrate how the proposed algorithm works, we ran a simulated environment using Matlab, where we considered a field of view  $\varphi = 180^\circ$ , and a range  $r = 20m$  for our remote gas sensor. Fig. 7 shows the environment setup (obstacle locations and gas source locations) and the robot's measurement configurations. The location of the artificial gas sources is denoted by the red squared markers.  $\pi_{\text{detect}}$  is shown as a series of green circular segments with angles and radius equal to the sensor's field of view and range respectively. Notice that at configuration 3, high concentrations are reported (since the robot is near a gas source). This triggers the computation of  $\pi_{\text{tomo}}$ , which is a re-planning process for exploitation. In our example,  $\pi_{\text{tomo}}$  corresponds to the red circular segments, for example configuration 4 when the first gas source is detected. After  $\pi_{\text{tomo}}$  is executed,  $\pi_{\text{detect}}$  is re-computed and those configurations that are no longer needed are discarded (gray markers in Fig. 7). Similarly, when a new gas source is detected at configuration 6, the computation of a new  $\pi_{\text{tomo}}$  is triggered, which leads to the suggestion of configuration 7 (in red) for exploitation purposes. The exploration process is thus concluded when the robot executes configuration 8 which corresponds to  $\pi_{\text{detect}}$ .



We have evaluated our adaptive sensor planning solutions in an indoor environment of size of  $X \times Y \text{m}$  where methane sources were placed at different locations. These methane sources consisted of transparent plastic flasks filled with methane. We used a robotic platform (Husky A-200) equipped with an actuated TDLAS and other sensing modalities for navigation such as a velodyne HDL-32E. We considered a field of view  $\varphi = 270^\circ$ , and a range  $r = 15\text{m}$ . Fig. 8 shows the computed gas distribution map from an exploration/exploitation run. The purple markers denote the location of the methane flasks and the estimated gas distribution map is shown as a series of markers coloured according to the estimated concentration. Higher concentrations are coloured with red shades while low concentrations are coloured with yellow shades. Notice that the algorithm predicts higher concentrations near the actual locations of the gas sources.



## D Sensor planning for communication coverage

To maintain a communication link between the human operator and the robotic platform, Smokebot developed a series of ruggedized wireless repeaters that are deployed as the mission is being conducted (T7.3) in order to extend the range of the Wireless (WLAN) network. However, it could be the case that the robot goes out of the WiFi range when in a mission. As part of the self preservation functionality (T5.2), the robot will continuously monitor radio frequency (RF) signal strength and augment the General Disaster Model with it.

To predict the connectivity of the network and to suggest a possible location to drop a repeater, Smokebot developed a ray-tracing-based algorithm that estimates the WLAN range of the network and extend it if needed by suggesting POIs where more repeaters could be dropped (D5.2).

Ray tracing is widely used in computer graphics to render high quality images: For each pixel on the screen, the path of the light is traced back into the scene it is coming from; the individual pixel is then colored in the color of the object(s) the light ray encounters. This method can not only be used to generate images, it is also used in physics to simulate the behavior of waves and particles.

Ray tracing is a suitable approach to simulate WiFi equipment since the estimation of WLAN coverage needs to be computed in real time and approaches that use, for example, the equations that describe the propagation of electromagnetic waves, could provide a subpar performance due to computational requirements. Related work, such as [12, 13] have shown that ray tracing can be used to simulate WiFi with a good level of accuracy. Moreover, commercial tools to plan wireless networks are based on ray tracing<sup>2</sup>.

We implemented the proposed ray-tracing-based algorithm for WiFi coverage in ROS. We modeled each repeater as a laser scanner device with a range that depends on the traversed objects. Thus, the scanner code was implemented in such a way that the projected rays do not stop on the first object they hit but instead, they keep track of the traveled distance and the number of hit objects. The maximum range is then adjusted according to the traversed objects. In addition, if another scanner is encountered this is recorded and the information can be used to create a map of connected network devices. The result of the modified ray tracing can be seen in Fig. 9. The area that is covered by the WiFi repeater in the middle is colored red. It can be seen that the signal reaches the furthest in the bottom of the image, while it is attenuated by walls in the other directions.

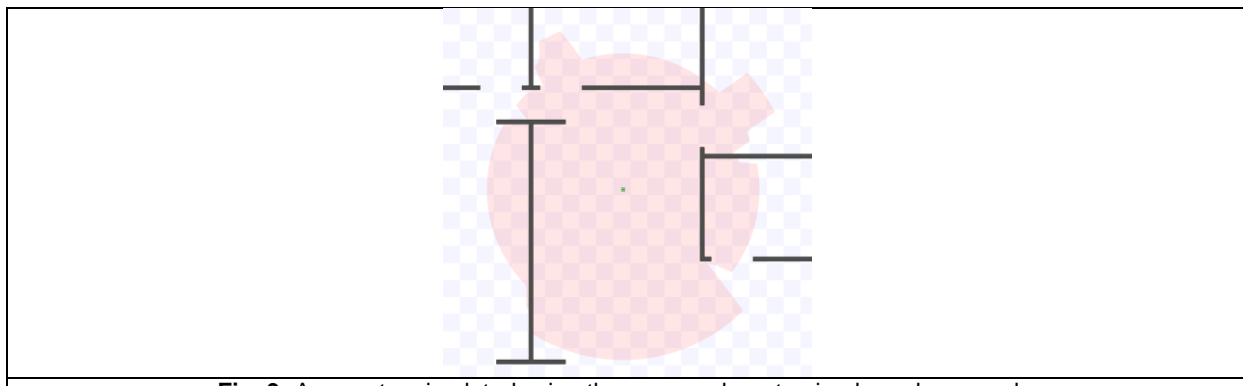


**Fig. 9:** A repeater simulated using the proposed ray-tracing-based approach.

Figs. 10(a) and 10(b) show how the proposed algorithm works. The algorithm was implemented as a ROS node that listens to the topics coming from the simulated repeaters currently in use. For each repeater, a polygon consisting of the translated points is kept updated, and to check if a point on the map is covered by the WiFi network one simply has to check if the point lies within one of these polygons. The algorithm also considers the input from the user in the form of the next position computed by the path planning algorithm. If the user commands the robot outside the area of coverage, a new WiFi repeater is placed early enough so that the robot always stays connected. Fig. 10(a) shows the coverage at the start of the exploration path and after it moves from its starting point in the lower left corner to the destination in the upper right corner Fig 10(b). Whenever the robot it is about to get

<sup>2</sup> <https://www.remcom.com/wireless-insite-em-propagation-software/>

outside the Wifi range, another repeater is dropped. The benefit of this approach is that it is completely independent of the specific path planner that is used.

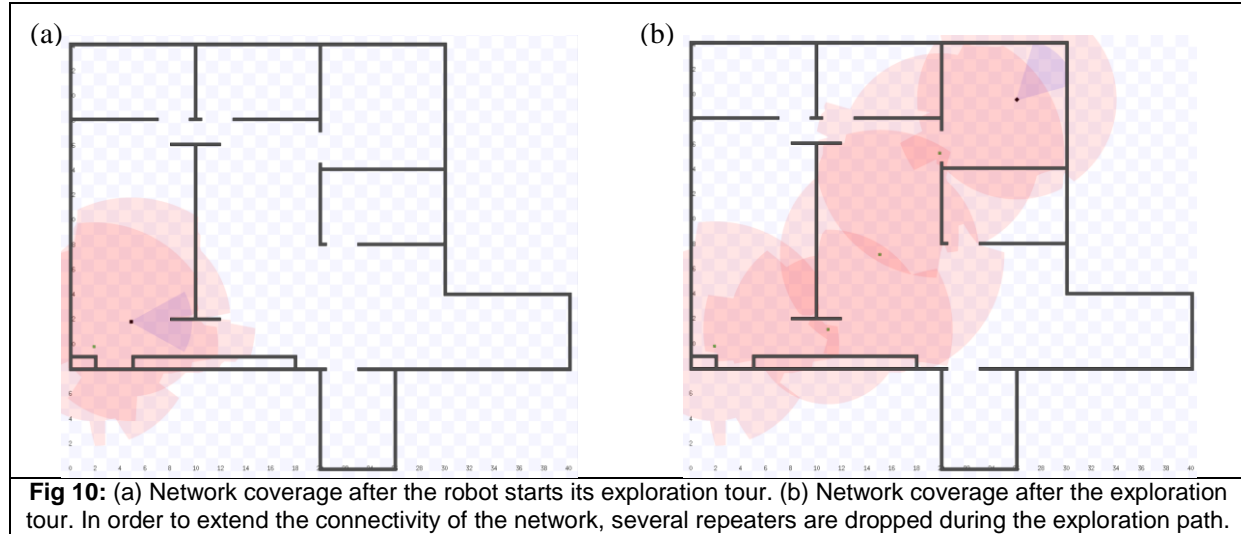


**Fig 10:** (a) Network coverage after the robot starts its exploration tour. (b) Network coverage after the exploration tour. In order to extend the connectivity of the network, several repeaters are dropped during the exploration path.

## E Summary and Outlook

In Smokebot we have developed different algorithms for sensor planning based on the sensor characteristics. More specifically, we developed algorithms for remote sensing, in-situ sensing and communication coverage. A key characteristic of Smokebot is that the human operator is in control of the exploration missions and thus, the sensor planning algorithms suggest new measurement locations as Positions Of Interest (POI) instead of controlling the robot's trajectory. It is up to the user operator (and the task that has higher priority at a given point) to decide where to move the robot.

For in-situ sensor planning, we explored two different approaches for gas source localization and gas distribution mapping. We first proposed a sensor planning algorithm that does not make any a-priori assumption about the gas dispersion (i.e. a model-free approach). This approach suggests POIs based on the variability of the gas measurements and airflow data and for non-visited locations, Gaussian extrapolation is used. This extrapolation model then allows to suggest POIs to explore the target area and to exploit the acquired information in order to detect the gas leaks. While the use of wind data could be perceived as a limitation of the algorithm in the Smokebot scenario, a possible solution is to use an isotropic Gaussian kernel. Regarding our model-based approach, we found that the performance. In addition, we proposed a model-based approach that relies on PDE to localize the gas sources and to map gas distribution. This algorithm proposes POIs based on hypotheses of where the gas source location might be (exploration) and areas where the uncertainty can be reduced (exploitation). In our hardware-on-the-loop evaluation, we found that the algorithm converges rapidly towards the location of the gas source and that the algorithm is rather accurate when localizing gas sources.

Regarding sensor planning for remote devices, we proposed an adaptive sensor planning for gas distribution mapping that first computes a set of POI for exploration (e.g. a given sensing coverage) and then, modifies the original plan as data is being collected in order to maximize a given performance metric (exploitation, in the form of gas map quality). The algorithm was tested with the task of gas distribution mapping with remote sensors. While gas distribution mapping with remote sensors is not part of the Smokebot scenario, the algorithm is flexible enough to address different remote sensing related applications, for example, the placement of thermal cameras or range sensors in

the environment. The algorithm presented in this document depends on parameters such as field of view ( $\varphi$ ) and range ( $r$ ). Such parameters can be set according to the remote sensor characteristics. Parameters such as  $n_{cov}$  (Equation C.1) denote the desired coverage (exploration) and it is not bound to the particular task of remote gas sensing. Similarly,  $n_{tomo}$  (Equation C.2) is a parameter that denotes a desired performance level. In the case of gas distribution mapping,  $n_{tomo}$  denotes the quality of the estimated maps. For a different application, a suitable metric can be used instead.

To conclude, we addressed sensor planning for the task of communication coverage. For this particular task, we implemented an ad-hoc algorithm that models the coverage of the individual repeaters as range sensors and considers the interference of obstacles in order to determine the overall coverage of the network. The proposed algorithm considers the estimated coverage and the next robot position (provided by the motion planning algorithm) in order to determine whether or not the robot is going out of range. If it is determined that the robot is moving outside the area of coverage, a repeater is dropped. While our ad-hoc algorithm diverges from the POI approach, it allows nevertheless for future developments. For example, it would be possible to provide the information about the network coverage to a specialized path planner that could then take this information into account and plan the route so it tries to stay in range of the Wifi.

## References

[1]	M. Schmuker, V. Bahr, and R. Huerta, "Exploiting plume structure to decode gas source distance using metal-oxide gas sensors", Sensor and Actuator B-Chemical, vol. 235, pp. 636-646, 2016
[2]	M. Reggente and A. J. Lilienthal, "Using Local Wind Information for Gas Distribution Mapping in Outdoor Environments with a Mobile Robot", in Proc. IEEE Sensors, pp. 1715-1720, 2009.
[3]	Roberts, P., and Webster, "Turbulent Diffusion. Environmental Fluid Mechanics Theories and Application", Reston, VA: ASCE Press,2002.
[4]	M. Demetriou, "Numerical investigation on optimal actuator/sensor location of parabolic PDEs," Proceedings of the 1999 American Control Conference, vol. 3, no. June, pp. 1722–1726, 1999.
[5]	F. Pukelsheim, Optimal Design of Experiments. John Wiley & Sons, Inc., 1993.
[6]	A. Alexanderian, N. Petra, G. Stadler, and O. Ghattas, "A-optimal design of experiments for infinite-dimensional Bayesian linear inverse problems with regularized l0-sparsification," SIAM Journal on Scientific Computing, vol. 36, no. 5, p. 27, 2013.
[7]	K. Kunisch, K. Pieper, and B. Vexler, "Measure Valued Directional Sparsity for Parabolic Optimal Control Problems," SIAM Journal on Control and Optimization, vol. 52, no. 5, pp. 3078–3108, jan 2014.
[8]	Strikwerda, J.C.: Finite Difference Schemes and Partial Differential Equations, 2 edn. Society for Industrial and Applied Mathematics, Philadelphia (2004)
[9]	M. E. Tipping, "Sparse Bayesian Learning and the Relevance Vector Machine," Journal of Machine Learning Research, 2001.
[10]	D. P. Wipf and B. D. Rao, "Sparse Bayesian learning for basis selection," Signal Processing, IEEE Transactions on, vol. 52, no. 8, pp. 2153–2164, 2004.
[11]	M. A. Arain, M. Trincavelli, M. Cirillo, E. Schaffernicht and A. J. Lilienthal. Global coverage measurement planning strategies for mobile robots equipped with a remote gas sensor. Sensors, 15(3):6845-6871, 2015
[12]	M. A. Arain, H. Fan, V. Hernandez Bennetts, E. Schaffernicht and A. J. Lilienthal. Improving Gas Tomography With Mobile Robots : An Evaluation of Sensing Geometries in Complex Environments. In 2017 ISOCS/IEEE International Symposium on Olfaction and Electronic Nose (ISOEN 2017) Proceedings 2017
[13]	T. R. S.Y. Seidel, „A ray tracing technique to predict path loss and delay spread inside buildings,“ 1992.
[14]	R. Valenzuela, „A ray tracing approach to predicting indoor wireless transmission,“ 1993.

## Appendices

# Exploration and Localization of a Gas Source with MOX Gas Sensors on a Mobile Robot - A Gaussian Regression Bout Amplitude Approach

Mikel Vuka<sup>1\*</sup>, Erik Schaffernicht<sup>2</sup>, Michael Schmuker<sup>3</sup>, Victor Hernandez Bennetts<sup>2</sup>, Francesco Amigoni<sup>1</sup> and Achim J. Lilienthal<sup>2</sup>

**Abstract**—Mobile robot olfaction systems combine gas sensors with mobility provided by robots. They relief humans of dull, dirty and dangerous tasks in applications such as search & rescue or environmental monitoring. We address gas source localization and especially the problem of minimizing exploration time of the robot, which is a key issue due to energy constraints. We propose an active search approach for robots equipped with MOX gas sensors and an anemometer, given an occupancy map. Events of rapid change in the MOX sensor signal (“bouts”) are used to estimate the distance to a gas source. The wind direction guides a Gaussian regression, which interpolates distance estimates. The contributions of this paper are two-fold. First, we extend previous work on gas source distance estimation with MOX sensors and propose a modification to cope better with turbulent conditions. Second, we introduce a novel active search gas source localization algorithm and validate it in a real-world environment.

## I. INTRODUCTION

Mobile Robot Olfaction (MRO) studies the combination of mobile robots with gas sensors to solve practical problems related to gas sensing. Among others, MRO systems perform gas discrimination, gas source localization (GSL), and gas distribution mapping. GSL can be of great importance for applications such as search and rescue missions, or environmental monitoring. Robotic solutions are especially favourable in dull, dirty or dangerous scenarios. When the gas of interest is harmful to humans, for example, it is indispensable to localize gas sources with a robot. The length of robot missions, however, is typically considerably limited by the available energy, both for ground and airborne robots. The challenges in GSL thus include importantly to find efficient navigation strategies that minimize the amount of time required for searching for a gas source.

In this paper, we present an active search GSL algorithm for a mobile robot, equipped with Metal-Oxide (MOX) gas sensors and a wind sensor. The robot searches a known environment (i.e., we assume that an occupancy map is given) for the gas source. The approach that we introduce estimates the gas source distance from the robot’s position and aims to minimize it by exploiting a model of the wind flow and how it affects the gas distribution.

<sup>1</sup>Dipartimento di Elettronica, Informazione e Bioingegneria, Politecnico di Milano, 20133, Milano, Italy

<sup>2</sup>Mobile Robotics & Olfaction Lab, Center of Applied Autonomous Sensor Systems (AASS), Örebro Universitet, SE-70182 Örebro, Sweden.

<sup>3</sup>University of Hertfordshire, School of Computer Science, College Lane, Hatfield, Herts AL10 9AB United Kingdom

\*Corresponding author mikel.vuka@mail.polimi.it

This work was funded in part by H2020-ICT project SmokeBot (645101).

The problem of gas source localization has been studied in the past two decades and there are several methods to approach it. In general, plume-tracking algorithms make use of wind flows (anemotaxis) and/or gas concentration (chemotaxis) to find a direction for the robot to follow. A broad group of algorithms try to mimic odor source localization performed by insects in nature [3], [4]. In these approaches the robots follow the gas plume in the upwind direction by making use of both anemotaxis and chemotaxis principles, whereas in our work we include an explicit source distance estimation in the process. For this estimation we draw upon recent works, which showed that the information conveyed by MOX sensors can be used to estimate the distance to a gas source in wind tunnel conditions [1]. Li et al. [6], [7] approach the problem by estimating the source location inside an area and then try to minimize this area. Some more complex algorithms model the location of the gas source with a probability distribution and then try to reduce its entropy [5]. These algorithms model the source location probabilistically, while we search the environment and build a probabilistic model of the source distance.

The contributions of this paper are two-fold. First, we introduce and validate a novel active search GSL approach. Second, we extend the work on gas source distance estimation, which was carried out in a wind tunnel [1]. We show results of the source distance estimation technique presented in [1] in real-world environments and introduce a modified version better suited to the task.

## II. PROBLEM DEFINITION AND APPROACH

We assume that the environment is known a priori and is not subject to change during a mission. The environment is represented as a Cartesian grid, thus obtaining a set  $M$  of  $N$  cells of identical size:  $M = \{x_1, \dots, x_N\}$ . We also assume that only one source of gas is present in the environment.

The robot is equipped with an array of six in-situ sensors. In order to measure wind speed and direction, the robot is equipped with an ultrasonic anemometer.

The robot moves between the centers of the cells. After each movement it records measurements of gas concentration and wind information for a certain amount of time in order to compute the source distance estimation. We define a function  $f : M \rightarrow \mathbb{R}^+$  to indicate the distance  $f(x)$  from a cell  $x \in M$ . The function  $f$  is unknown a priori and is updated from noisy measurements. From the measurements made in visited areas, the robot estimates values of the function  $f$  in unvisited areas of the environment and uses this knowledge

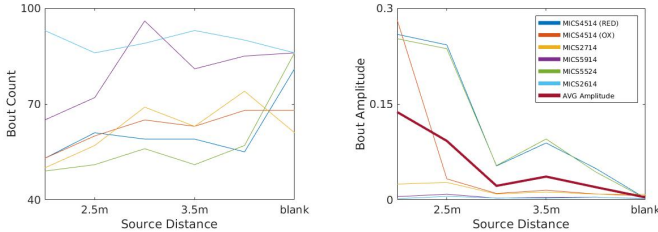


Fig. 1: Bout count and amplitude for each sensor vs. distance to the gas source at 0.1 m/s wind speed.

to decide where to navigate next in order to improve the estimation in an efficient way. The estimation of the source distance is thus performed online, as the robot visits the environment. The approach proposed in this paper consists in the repetition of the following steps: acquire sensor data from the current position, compute the source distance estimation, estimate  $f(x)$ , and finally move the robot to the next position selected by the search strategy. The two main modules of our system, namely source distance estimation and search strategy, are described in the following.

### III. SOURCE DISTANCE ESTIMATION

One of the crucial steps of our approach is the detection of the *bouts* of the signal, i.e., portions of the filtered signal where the amplitude is rising. In [1], it is reported that there is a strong correlation between the number of bouts and the distance to the gas source: the higher the bout count, the closer the sensor to the gas source.

To detect the bouts, a cascaded filtering approach is used to detect fast transients in the sensor signal [1]. A low-pass filter is first used in order to remove high-frequency noise. This is done by applying a Gaussian convolution with  $\sigma_{smooth} = 0.3s$ . On the smoothed signal, a differential convolution is applied to show differences between pairs of samples and see the amplitude changes. Finally, the signal undergoes an exponentially-weighted moving average filter with a half life  $\tau_{half} = 0.4s$ . The operation that yields the filtered time series  $y_t$  from the low-pass filtered  $z_t$  can be expressed by the following equation:

$$y_t = (1 - \alpha) * y_{t-1} + \alpha * z_t \quad (1)$$

where  $\alpha = 1 - \exp \frac{\log(0.5)}{\tau_{half} \Delta t}$  and  $\Delta t$  is the time step in the equation. Bouts of rising amplitude can be identified on the differential of the filtered signal ( $y'_t$ ). The presence of a bout is characterized by  $y'_t$  being equal to or greater than zero.

The bout method in [1] was evaluated only inside a wind tunnel, while we are considering open environments. The gas plume was generated through evaporation of propanol placed inside an open plastic container. A constant wind flow was generated with a fan placed near the gas source. The bout detection was tested with low wind speeds (0.1 m/s to 0.4 m/s). The propanol container was placed in between the robot and the fan at different distances from the robot in 6 different locations in the range from 2 to 4 meters. The sampling rate of the sensors was set to 74 Hz and the sensing time of the robot was 135 seconds, obtaining a gas concentration signal

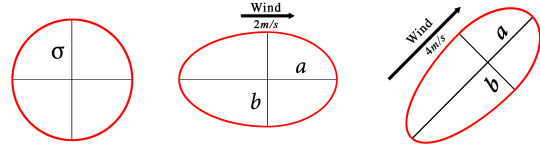


Fig. 2: Influence of the wind speed and direction on the shape of the kernel. The ellipse is rotated according to the wind direction. The semimajor axis  $a$  is stretched in the upwind direction and shrunk in the downwind direction according to the wind speed.  $\sigma$  represents the spatial scale of the kernel.

with a total of 10,000 samples per location for the bout detection algorithm. Experiments were repeated 6 times.

Our experiments show that the bout count gives mixed results in this scenario and cannot be used to reliably estimate the distance to the gas source. In some cases it can be seen that the bout count even increases with distance. From the analysis of the gas concentration signal, we noted, however, that the amplitude of the bouts tends to decrease with distance, making it possible to estimate the source distance. The distance is thus estimated for each sensor as the mean value of the amplitudes of all the bouts. Our results (Fig. 1) actually show that the average bout amplitude is a good indicator of the distance to the gas source. In some cases, when moving away from the source by 0.5 m the average amplitude slightly increases. However, in most cases, the average bout amplitude decreases when moving away from the source for more than 1 m.

In the experiments performed in outdoor environments the wind flow conditions were not stable, resulting in the wind changing direction very often. Moreover, the wind speed was much higher than in indoor environments (about 1 m/s). Because of the high wind speed, the transients of the signal are too short and the sensors cannot resolve them, resulting in failure to detect the bouts. Overall, the sensors used in our experiments were able to reliably estimate the source distance in wind speeds up to 0.3 m/s.

### IV. SEARCH STRATEGY

#### A. Algorithm

We model the average bout amplitude function  $f(x)$  (which is related to the distance from the robot to the gas source) as a Gaussian process with kernel function  $k : M \times M \rightarrow \mathbb{R}^+$ . Since, in realistic environments, advection dominates gas dispersal we use the upwind direction to direct  $f(x)$  towards the gas source. This then favors exploration in upwind directions. We include wind information using a radial kernel, stretched according to the wind speed and rotated according to the wind direction as in [2], see Fig. 2:

$$k(x, x') = \exp -\sqrt{(x - x')^T \Sigma^{-1} (x - x')} \quad (2)$$

where  $\Sigma$  is the 2D covariance matrix of the Gaussian.

The kernel in Eq. 2 corresponds to the assumption that positions in upwind direction have a bout amplitude similar

to the measurement point. It also expresses the exploitation component of the exploration strategy, which leads the robot to follow a gas plume. The bout amplitude estimation at an unvisited location  $x_*$  and the a posteriori variance are computed respectively as:

$$\begin{aligned}\bar{f}_* &= k_*^T [K + \sigma_n^2 I]^{-1} y \\ V[f_*] &= k(x_*, x_*) - k_*^T [K + \sigma_n^2 I]^{-1} k_*\end{aligned}\quad (3)$$

where  $k_*$  and  $K$  are abbreviations respectively for  $k(x_*, X)$  and  $k(X, X)$  and  $X$  is the set of visited cells.

The direction towards the next sensing position is computed as a trade-off between exploration of unvisited areas (following the variance gradient) and exploitation (following the direction to the highest bout amplitude estimate). The robot moves to the next position by following a direction  $\theta$  for a step size  $\rho$ . The direction  $\theta$  is sampled from the following Gaussian distribution:

$$p(\theta) = \begin{cases} \exp \frac{-(\theta - \theta_m(s))^2}{\sigma_m^2} & \text{if } R > \tau \\ \exp \frac{-(\theta - \theta_v(s))^2}{\sigma_v^2} & \text{otherwise} \end{cases} \quad (4)$$

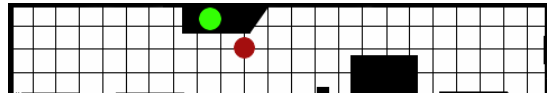
where  $s$  is the iteration step,  $\theta_m(s)$  is the direction to the highest bout amplitude estimation,  $\theta_v(s)$  is the direction to the highest variance,  $\tau$  is the trade-off parameter and  $R \in [0, 1]$  is a random variable. At the beginning  $\tau$  is set to 1. During the first steps of the mission the trade-off favors exploration and the robot moves towards unknown areas. After each step of the algorithm, the trade-off parameter decays to slightly lean more towards exploitation. If exploitation is favored, the robot follows the direction to the highest bout amplitude estimation. When the a posteriori variance is low enough (i.e.,  $\tau$  goes under a threshold), the algorithm terminates by declaring the position where the highest bout amplitude estimate is found as the final one.

### B. Experimental results

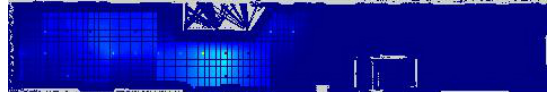
Experiments with a Clearpath Husky A200 robot were performed in a 22m x 4m indoor corridor.

The sensory function for Gaussian regression was derived from the bout amplitudes of the all signals of the sensor array. The estimation of the source distance is not always accurate if derived from a single sensor, especially the low resistance sensors were found to be not very reliable. The bout amplitude from the high resistance sensors, on the other hand, showed only small changes with distance. Therefore, the distance was estimated using all sensors. More specifically, for each sensing operation, the average bout amplitude for each sensor is calculated, then the six values are averaged together to have the final value. In this way, the effects of the sensors are balanced in order to get a good estimation. The occupied cells in the occupancy grid are considered to have a bout amplitude equal to zero.

We consider an experiment successful if the robot chooses as the final position the reachable cell nearest to where the gas source is placed, along the wind direction (Fig. 3). From a total of 12 complete experiments that were run, 8 were



(a) Grid map of the environment: The black cells indicate obstacles. The green circle indicates the gas source and the red circle the final position of the robot.



(b) The mean estimate map: The dark blue regions map areas with low bout amplitude estimates, whereas the light blue indicates high mean values.

Fig. 3: Results of an experiment in which the wind was flowing towards the south-east direction.

successful in identifying the proper final position, giving our method a 67% success rate. Reasons that could explain the failed experiments include the high wind speeds (which lead to bouts that cannot be resolved) and that the plane in which the robot sampled gas concentrations was at a substantially lower height than the gas source.

### V. CONCLUSIONS

In this paper we introduced an integrated GSL and exploration approach that uses a mobile robot equipped with MOX sensors and a wind sensor. The proposed solution exploits the bout amplitude of the concentration signal and drives the robot towards areas where its value is expected to be maximized. Experimental results show that the bout amplitude of the signal is a good estimator of the source distance. The proposed search strategy performed with a success rate of 67% in indoor environments, identifying reachable areas near the gas source.

A possible improvement of the work done in this paper would be to consider scenarios with multiple gas sources. The robot then estimates the number of sources and the distance to the closest one. Possible extensions would be to study the bout amplitude response of different gases and try to learn detection thresholds in order to declare the presence of a gas source.

### REFERENCES

- [1] M. Schmuicer, V. Bahr, and R. Huerta, “Exploiting plume structure to decode gas source distance using metal-oxide gas sensors”, *Sensor Actuat B-Chem*, vol. 235, pp. 636-646, 2016.
- [2] M. Reggente and A. J. Lilienthal, “Using Local Wind Information for Gas Distribution Mapping in Outdoor Environments with a Mobile Robot”, in *Proc. IEEE Sensors*, pp. 1715-1720, 2009.
- [3] Y. Kuwana, I. Shimoyama, and H. Miura, “Steering control of a mobile robot using insect antennae,” in *Proc. IROS*, pp. 530-535, 1995.
- [4] Y. Kuwana and I. Shimoyama, “Pheromone-guided mobile robot that behaves like a silkworm moth with living antennae as pheromone sensors.,” in *Proc. IROS*, pp. 924-933, 1998.
- [5] M. Vergassola, E. Villermaux, B. I. Shraiman, “Infotaxis’ as a strategy for searching without gradients”, *Nature*, vol. 445, pp. 406-409, 2007.
- [6] J.-G. Li, Q.-H. Meng, Y. W., and M. Zeng, “Odor source localization using a mobile robot in outdoor airflow environments with a particle filter algorithm”, *Auton Robot*, vol. 30, pp. 281-292, 2011.
- [7] J.-G. Li, Q.-H. Meng, F. Li, M. Zeng and D. Popescu, “Mobile Robot based Odor Source Localization via Particle Filter” in *Proc. CDC/CCC December 16-18, 2009*.

## Manuscript Details

<b>Manuscript number</b>	ROBOT_2018_341
<b>Title</b>	Model-based Gas Source Localization Strategy for a Cooperative Multi-Robot System - A Probabilistic Approach and Experimental Validation Incorporating Physical Knowledge and Model Uncertainties
<b>Article type</b>	Research Paper
<b>Abstract</b>	
Sampling gas distributions by robotic platforms in order to find gas sources is a favorable approach to alleviate threads for a human operator. Even so, different sampling strategies for robotic gas exploration exist, in this paper we investigate the benefit that could be obtained by incorporating physical knowledge about the gas dispersion. We consider the problem of exploring a gas diffusion process using a multi-robot system. The physical behavior of the diffusion process is modeled using a PDE which is integrated into the exploration strategy. It is assumed that the diffusion process is driven by only a few spatial sources at unknown locations with unknown intensity. The objective of the exploration strategy is to guide the robots to informative measurements location and by means of concentration measurements estimate the source parameters, in particular, their number, locations and magnitudes. To this end we propose a probabilistic approach towards PDE identification under sparsity constraint using factor graphs and a message passing algorithm. Moreover, the message passing schemes permits efficient distributed implementation of the algorithm specially suitable for a multi-robot system. We designed a experimental setup that allows us to evaluate the performance of the exploration strategy in hardware-in-the-loop experiments as well as in experiments with real ethanol gas under lab conditions. The results show that the proposed exploration approach accelerates the identification of the source parameters and outperforms systematic sampling.	
<b>Keywords</b>	robotic Exploration; gas source localization; multi-agent-System; partial differential equation; mobile robot olfaction; sparse Bayesian learning; factor graph; message passing
<b>Taxonomy</b>	Sensor System, Robotics
<b>Corresponding Author</b>	Thomas Wiedemann
<b>Corresponding Author's Institution</b>	German Aerospace Center
<b>Order of Authors</b>	Thomas Wiedemann, Dmitriy Shutin, Achim Lilienthal
<b>Suggested reviewers</b>	Ali Marjovi, Silvia Ferrari, Qinghao Meng

## Submission Files Included in this PDF

### File Name [File Type]

Cover\_Letter.pdf [Cover Letter]

RAS\_2018.pdf [Manuscript File]

Biography.pdf [Author Biography]

Wiedemann.jpg [Author Photo]

Shutin.jpg [Author Photo]

Lilenthal.jpg [Author Photo]

To view all the submission files, including those not included in the PDF, click on the manuscript title on your EVISE Homepage, then click 'Download zip file'.

## Research Data Related to this Submission

There are no linked research data sets for this submission. The following reason is given:  
Data will be made available on request

**Submission for the RAS Special Issue of selected paper from ECMR 2017**

Dear,

As corresponding editor of the Special Issue of selected paper from ECMR 2017 in the Journal “Robotics and Autonomous Systems” (RAS) I am submitting to you a paper of Dmitriy Shutin, Achim J. Lilienthal and mine, entitled “Model-based Gas Source Localization Strategy for a Cooperative Multi-Robot System - A Probabilistic Approach and Experimental Validation Incorporating Physical Knowledge and Model Uncertainties”.

Please accept it as a candidate for publication in the RAS Journal.

This manuscript is a substantial extension of our previous conference paper “Probabilistic modeling of gas diffusion with partial differential equations for multi-robot exploration and gas source localization” submitted to the European Conference on Mobile Robots (ECMR), 2017. This manuscript provides a more comprehensive, more detailed theoretical description of our approach compared to the conference paper.

Further, we now present results from experiments with real ethanol gas in a laboratory environment which was not part of the conference paper before.

Apart from the ECMR submission, this paper is our original unpublished work and it has not been submitted to any other journal for review.

I am looking forward to hear from you.

Yours sincerely,

Thomas Wiedemann

---

**Deutsches Zentrum für Luft- und Raumfahrt e.V. (DLR)**  
German Aerospace Center  
Institute of Communications and Navigation | Oberpfaffenhofen | 82234 Wessling | Germany

**M.Sc. Thomas Wiedemann**

Telephon 08153 28-4214 | Telefax 08153 28-1871 | [thomas.wiedemann@dlr.de](mailto:thomas.wiedemann@dlr.de)

[DLR.de](http://DLR.de)

# Model-based Gas Source Localization Strategy for a Cooperative Multi-Robot System - A Probabilistic Approach and Experimental Validation Incorporating Physical Knowledge and Model Uncertainties

Thomas Wiedemann<sup>a,\*</sup>, Dmitriy Shutin<sup>a</sup>, Achim J. Lilienthal<sup>b</sup>

<sup>a</sup>*German Aerospace Center, Oberpfaffenhofen, Germany*

<sup>b</sup>*Centre for Applied Autonomous Sensor Systems, Örebro University, Örebro, Sweden*

---

## Abstract

Sampling gas distributions by robotic platforms in order to find gas sources is a favorable approach to alleviate threads for a human operator. Even so, different sampling strategies for robotic gas exploration exist, in this paper we investigate the benefit that could be obtained by incorporating physical knowledge about the gas dispersion. We consider the problem of exploring a gas diffusion process using a multi-robot system. The physical behavior of the diffusion process is modeled using a Partial Differential Equation (PDE) which is integrated into the exploration strategy. It is assumed that the diffusion process is driven by only a few spatial sources at unknown locations with unknown intensity. The objective of the exploration strategy is to guide the robots to informative measurements location and by means of concentration measurements estimate the source parameters, in particular, their number, locations and magnitudes. To this end we propose a probabilistic approach towards PDE identification under sparsity constraint using factor graphs and a message passing algorithm. Moreover, the message passing schemes permits efficient distributed implementation of the algorithm specially suitable for a multi-robot system. We designed

---

\*Corresponding author

Email addresses: [thomas.wiedemann@dlr.de](mailto:thomas.wiedemann@dlr.de) (Thomas Wiedemann),  
[dmitriy.shutin@dlr.de](mailto:dmitriy.shutin@dlr.de) (Dmitriy Shutin), [achim.lilienthal@oru.se](mailto:achim.lilienthal@oru.se) (Achim J. Lilienthal)

a experimental setup that allows us to evaluate the performance of the exploration strategy in hardware-in-the-loop experiments as well as in experiments with real ethanol gas under lab conditions. The results show that the proposed exploration approach accelerates the identification of the source parameters and outperforms systematic sampling.

*Keywords:* robotic exploration, gas source localization, multi-agent-system, partial differential equation, mobile robot olfaction, sparse Bayesian learning, factor graph, message passing

---

## 1. Introduction

In this paper we consider the task of finding gas sources, e.g. gas leaks, by exploring the resulting gas dispersion with autonomous robots. The proposed approach may be applied in technical accident or disaster response scenarios,  
5 where toxic or explosive material is leaking. In such cases localizing the sources is of high interest and relevant to safety. However, for civil protection agencies searching for toxic gas leaks in an already contaminated environment implies threats for human operators. Thus, employing robotic platforms in those scenarios might be beneficial with respect to safety aspects. Moreover, robots with  
10 a certain level of autonomy simplify the work of a human operator, as compared to just teleoperated platforms. For example a robot can instantaneously interpret the collected data and decide based on them, which otherwise would require a trained operator or specialist. Following this motivation, we propose to make use of robotic platforms which, equipped with gas sensors, can sample  
15 the gas concentration in the environment and process the data in an automated fashion in order to localize gas sources.

Moreover, a multi-robot system is of advantage, since it is capable of taking measurements at different locations at the same time. This is of advantage for analyzing the dispersion process, since the gas dispersion is dynamic, and  
20 the time-variant nature of gas dispersion is an important property, that should be taken into account [1]. For example, a single concentration measurement

contains no information about the gradient of the concentration, which is an important property since it may lead to a gas source. Only after exploring some extended space, it is possible to get some directional information about the  
25 gas concentration. Besides, a multi-robot system has additional advantages:  
i) multiple robots can achieve the exploration task faster; ii) a multi-robot system is more robust, since it possesses natural redundancies; and finally iii)  
the individual robots can make use of synergies, e.g. share the computational costs of algorithms.

30 However, in order to guide the robots to informative measurement locations, an exploration strategy is needed. The use of robotic platforms for gas source localization, plume tracking or gas distribution mapping in general is an active research field and a lot of different strategies can be found in the literature, distinguishable by different categories. For an overview of different approaches and  
35 terminology we refer the reader to [2], [3] and [4]. One possibility to categorize exploration strategies for gas mapping or source localization are predefined vs. reactive (sometimes also called adaptive) strategies. For example both concepts are investigated in [5]. While a predefined strategy follows a plan or trajectory that was defined beforehand, a reactive strategy reacts to current measurements  
40 and adjusts its plans accordingly. For gas distribution mapping with the goal to measure everywhere, a predefined strategy that ensures full coverage of the area may be the method of choice. However, for gas source localization reactive strategies can be faster, as will be shown in this paper.

Since finding gas sources is also a challenge for animals like moths, beetles  
45 or bacteria, exploration strategies are often bio inspired, e.g. [6],[7]. These exploration strategies rely on local concentration gradients to move towards a gas source. Those approaches can be group together under the term chemotaxis. More advanced approaches, sometimes referred to as infotaxis, do not purely rely  
50 on concentration gradients, but are more information-based or entropy driven [8],[9]. Moreover, additional knowledge about the environment or constraints could be utilized for the exploration strategy. For example the search for a gas source could be supported by observations of the current wind field [10]

(anemotaxis). Or information about obstacles could be used, as done in [11].

In general, exploiting model assumptions about the gas dispersion enables  
55 the use of higher level strategies. Here high level strategy means path planning  
and way point navigation to control the robot, in contrast to a low level controller  
coupling the sensor signals directly to the motors, e.g. Braitenberg style  
[3]. In this paper we also propose to use a model-based approach to design an  
adaptive exploration strategy. A common way to model the process of a gas  
60 dispersion or the plume dynamics is to use PDEs [12],[13]. In this context the  
exploration or sampling problem is closely related to optimal sensor placement  
techniques. In the literature, some approaches consider this as an observer de-  
sign problem. In those cases an observer performance is optimized by adapting  
the sensor location, e.g. in [14] or [12] to estimate a distributed process de-  
65 scribed by a PDE. From another perspective, the sampling problem could be  
treated as an optimal experimental design problem [15]. More details on these  
topics can be found in [16], where the author gives an introduction to optimal  
sensor location and experimental design problems. To sum up, from our point  
of view a PDE seems a very useful way to put physical knowledge about the gas  
70 dispersion into a exploration strategy. Therefore, we follow this idea in the here  
presented approach. Unfortunately, model-based approaches for designing high  
level sampling strategies for gas exploration are mostly evaluated in simulation  
and not in real world experiments. So it is unclear if those approaches also work  
in real world scenarios where the model assumption may not hold. Therefore,  
75 we propose to use a probabilistic framework to be able to quantify also uncer-  
tainties in our model assumptions and hopefully get a more robust system. In  
general, a probabilistic or statistical view is also a contemporary and relevant  
research topic in the context of gas distribution mapping [17, 18]. Moreover,  
a probabilistic treatment enables to quantify informativeness of possible mea-  
80 surements locations [19]. Based on that we follow the idea of an uncertainty or  
entropy driven [20] exploration strategy.

This article is a substantial extension of a previous conference paper [21]. It  
provides a comprehensive, more detailed description of our approach than [21]

and presents real world experiments. The used methods and theory for modeling the PDE in a probabilistic framework and the algorithms for a distributed implementation were firstly introduced in [22].

The main focus of the presented approach is the gas source localization task. Our approach does not rely on any assumption about the sources' strengths, the sources' positions or even the exact number of sources. We only assume a sparse distribution of sources. In other words, we do not know the exact number of sources, but we expect that there are only a few of them. For the gas source localization task, the presented adaptive exploration strategy for the multi-robot system is based on a mathematical model of the gas dispersion. This PDE is described in Section 2. By means of the model we can infer the location of the gas sources based on gas concentration measurements taken by multiple robots. Further, the model is transferred to a probabilistic formulation as shown in Section 3. The probabilistic framework provides us with tools (i) to introduce the sparsity assumption about the source distribution and (ii) to quantify the spatial uncertainty about the gas and source distribution. To make use of synergies in the multi-agent-system Section 4 presents a Message Passing (MP) algorithm to perform all calculations in a distributed fashion. The actual exploration procedure grounded on the uncertainty quantification in our probabilistic model is explained in Section 5. This strategy guides the robots to their measurement locations. In contrast to the greedy algorithm in [22] where the robots only consider their direct neighborhood for a new measurement, in this paper robots possess a global view of the whole environment.

The main contribution of this work compared to our previous work is the evaluation of the presented approach in experiments presented in Section 6 and Section 7. In general, it is difficult to evaluate gas distribution exploration in realistic experiments due to the difficulty of measuring ground truth gas concentrations. In addition, interesting gas distributions for realistic applications may be of toxic nature and dangerous to handle. To overcome those issues we evaluated the approach in two steps: First, we tested the exploration strategy in hardware-in-the-loop experiments, where we employed a real multi-robot sys-

<sup>115</sup> tem but only virtually simulated the gas dispersion. This simulation provides us with ground truth data and facilitates reproducibility of the experiments. Second, to ensure that the approach is able to cope with model uncertainties we tested the approach in a real world experiment under lab conditions with ethanol as a toy gas.

<sup>120</sup> **2. Process Model**

In this work we consider an exploration of a gas diffusion process. In general, true physical mechanisms behind gas propagation are quite complex. Nonetheless, models exists that can “approximate” gas dynamics sufficiently well. Here we make use of such a model that describes spatial gas dynamics using a PDE.  
<sup>125</sup> More precisely, we approximate the gas propagation by the diffusion equation. Hereby, we neglect other effects like advection or turbulence.

Let us consider an exploration of a gas diffusion process in a bounded spatial region  $\Omega \subset \mathbb{R}^2$  over a some time interval  $T \in \mathbb{R}_+$ . A 2-dimensional gas diffusion process can be modeled with a linear parabolic PDE as follows

$$\frac{\partial f(\mathbf{x}, t)}{\partial t} - \kappa \Delta f(\mathbf{x}, t) = u(\mathbf{x}, t), \quad \mathbf{x} \in \Omega, t \in T, \quad (1)$$

where  $f(\mathbf{x}, t) : \Omega \times T \mapsto \mathbb{R}$  is a space- and time-variant function that represents gas concentration at location  $\mathbf{x}$  and at time  $t$ . Parameter  $\kappa$  in (1) is a gas diffusion coefficient. The right-hand side  $u(\mathbf{x}, t) : \Omega \times T \mapsto \mathbb{R}$  of (1) is interpreted as a gas source distribution. In particular, it describes the source strength (or intensity) of inflow at location  $\mathbf{x}$  and time  $t$ . Let us re-iterate that (1) is used as an approximation to the macroscopic gas dispersion caused by different complex physical mechanism.  
<sup>130</sup>

Both functions  $f(\mathbf{x}, t)$  and  $u(\mathbf{x}, t)$  are unknown. Our exploration aims at estimating both functions from measurements performed by individual agents. We will assume that measurements are performed by agents according to following model

$$y(\mathbf{x}, t) = f(\mathbf{x}, t) + \epsilon(\mathbf{x}, t), \quad (2)$$

i.e., we measure a value of a gas concentration perturbed by additive noise  
<sup>135</sup>  $\epsilon(\mathbf{x}, t)$  at location  $\mathbf{x}$  and time  $t$ . This model reflects many common gas sensors measurements (e.g., Metal Oxide (MOX) sensors or Photoionization detectors (PIDs)). As we see, the information about  $f(\mathbf{x}, t)$  is acquired directly by means of noisy gas concentration measurements. In contrast, the source distribution  
<sup>140</sup>  $u(\mathbf{x}, t)$  is hidden and must be inferred from measurements indirectly using some inference procedure.

To enable the probabilistic treatment of the exploration problem, we numerically approximate the space- and time-continuous system (1) with a discrete equivalent. Specifically, we use Finite Difference Method (FDM) [23] for this purpose. Although other, more advanced methods exist for this approximation,  
<sup>145</sup> the chosen discretization method is simple and illustrates well the proposed methodology. The investigations on the choice of discretization or the use of finite elements instead of finite differences are left outside the scope of this paper, despite the fact that they do impact the numerical approximation quality (see for example [24]).

<sup>150</sup> To discretize the time, we consider the system at discrete time intervals  $t = nT_s$ , with  $n \in \mathbb{N}_0$  and a sampling period  $T_s$ . The discretization in space is done as follows. The exploration domain  $\Omega$  is divided into  $C$  smaller subdomains  $\Omega_c$ ,  $c = 1, \dots, C$ , which form a grid with  $I$  rows and  $J$  columns, so that  $C = IJ$ . For simplicity and without loss of generality, we use quadratic cells. The functions  
<sup>155</sup>  $f(\mathbf{x}, t)$  and  $u(\mathbf{x}, t)$  can then be represented by discrete vectors  $\mathbf{f}[n] \in \mathbb{R}^C$  and  $\mathbf{u}[n] \in \mathbb{R}^C$  containing the concentration values and source strengths for each grid cell at time instance  $n$ . Note that during a time instance and within a grid cell the concentration values and source strengths are considered as constant.

Based on the discretization, the FDM simply replaces the differential operators in (1) by appropriate finite differences. Thereby, we obtain a system of linear equations as an numerical approximation of the PDE (1). More precisely, we get one equation for each sub-domain  $\Omega_c$ , i.e. each grid cell  $c = 1, \dots, C$ . This are residuals set to zero and representing a relation between the concentration  $f_c[n]$  of considered cell and its four spatial neighbors  $f_{c-1}[n], f_{c+1}[n],$

$f_{c-J}[n]$ , and  $f_{c+J}[n]$  as well as the source strength  $u_c[n]$  (inflow) in the cell and the concentration  $f_c[n - 1]$  of the previous time stamp:

$$r_c(f_c[n], f_{c-1}[n], f_{c+1}[n], f_{c-J}[n], f_{c+J}[n], f_c[n - 1], u_c[n]) = 0 \quad (3)$$

(for a more detailed formulation see [22]).

160 Let us remark that after the discretization, the source distribution  $u(\mathbf{x}, t)$  is represented by a vector  $\mathbf{u}[n]$ , with each element corresponding to the source strength (or intensity) in a particular cell. Thus our assumption that sources are sparsely distributed in the domain  $\Omega$ , means that the vector  $\mathbf{u}[n]$  is sparse in a sense that most of its entries are zero. The number and the index of nonzero 165 entries in  $\mathbf{u}[n]$  reflect the number and locations of the active gas sources, which we are interested to find.

Now consider  $K$  agents which explore  $\Omega$  by means of sampling the gas concentration process  $f(\mathbf{x}, t)$  according to (2). By collecting the measurements  $y_k[n]$  of individual agents in a vector  $\mathbf{y}[n] = [y_1[n], \dots, y_K[n]]^T$ , we can represent the measurement performed by the agents as

$$\mathbf{y}[n] = \mathbf{M}[n]\mathbf{f}[n] + \boldsymbol{\epsilon}[n]. \quad (4)$$

Here  $\mathbf{M}[n] = [\mathbf{m}_1, \dots, \mathbf{m}_K]^T$  is a spatial  $K \times C$  sampling matrix. Each vector  $\mathbf{m}_k[n] \in \mathbb{R}^C$ ,  $k = 1, \dots, K$ , is defined as a zero vector except one element that equals 1 at an entry that corresponds to the spatial cell  $c$  measured by the agent  $k$  at time  $n$ .

170 Finally, we assume the additive noise process  $\boldsymbol{\epsilon}[n]$  in (4) to be spatially and temporally white and normally distributed with zero mean and precision (a reciprocal of the variance)  $\tau_m$ , i.e.,  $\boldsymbol{\epsilon}[n] \sim N(\mathbf{0}, \tau_m^{-1}\mathbf{I})$ .

### 3. Probabilistic Framework

175 Our motivation for using a probabilistic formulation of the gas diffusion model is twofold. First, as we will see, this formulation permits us to account for a possible model mismatch between the actual gas dispersion process and

the used PDE model. Second, it will allow us to quantify the uncertainty of the explored processes in different regions of the domain  $\Omega$ . This property forms the  
<sup>180</sup> basis for our exploration strategy. In particular, we use information-theoretic tools to quantify uncertainties (see Section 3.2 for more details).

In the probabilistic setting the gas concentration vectors  $\mathbf{f}[n]$  and source strength vectors  $\mathbf{u}[n]$  (or rather the entries in these vectors) are treated as random variables. The underlying probabilistic structure will be explained in  
<sup>185</sup> the following.

### 3.1. Bayesian Formulation

As a first step, we relax equation (3). In particular, we assume that (3)  
is allowed to deviate from zero. This deviation – the residual of a grid cell – is a normally distributed random variable with zero mean and precision  $\tau_s$ .  
<sup>190</sup> These residuals are independent and identically distributed for all grid cells in  $\Omega$ . The latter assumption is reasonable since (3) is valid locally independently of other sub-regions. The role of  $\tau_s$  is to regulate our trust in the model: with  $\tau_s \rightarrow \infty$  we recover the deterministic case, which encodes the assumption that the dispersion process is accurately represented by (1). For small  $\tau_s$  we allow  
<sup>195</sup> the dispersion process to deviate from the model (1) and thus “tolerate” other dynamical effects that are not represented with a pure diffusion. This relaxation is a nice feature of the presented approach, since we are to parametrize our trust in the model by a single scalar value with a physical interpretation.

Under the above assumptions and using (3), we can now define the conditional Probability Density Function (PDF) of the gas concentration distribution  $\mathbf{f}[n]$  at time  $n$  as

$$p(\mathbf{f}[n] | \mathbf{f}[n-1], \mathbf{u}[n]) \propto \prod_{c=1}^C e^{-\frac{\tau_s}{2}(r_c(f_c[n], f_{c-1}[n], f_{c+1}[n], f_{c-J}[n], f_{c+J}[n], f_c[n-1], u_c[n]))^2}. \quad (5)$$

In a similar way the measurement model is casted in a probabilistic setting. Based on (4) and the assumed Gaussian noise characteristics we can formulate

the gas concentration likelihood function as follows:

$$p(\mathbf{y}[n]|\mathbf{f}[n]) \propto e^{-\frac{\tau_m}{2} \|\mathbf{M}[n]\mathbf{f}[n] - \mathbf{y}[n]\|^2} \propto \prod_{k=1}^K e^{-\frac{\tau_m}{2} (\mathbf{m}_k[n]^T \mathbf{f}[n] - y_k[n])^2}. \quad (6)$$

To complete the probabilistic formulation of our model, we also need to  
 200 specify two prior PDFs: an initial gas concentration  $\mathbf{f}[0]$  and a source prior  
 $p(\mathbf{u}[n]).$

The source prior  $p(\mathbf{u}[n])$  is a mechanism that we use to incorporate our  
 prior assumptions about the source sparsity. In order to encode this sparsity  
 assumption we appeal to Sparse Bayesian Learning (SBL) techniques [25]. This  
 205 approach we first proposed in [22]. In the following we give a short summary,  
 for a better understanding we refer the reader to [22] for more details.

Sparsity is introduced through construction of a hierarchical prior  $p(\mathbf{u}[n], \boldsymbol{\gamma}[n]),$   
 which is parameterized with hyper-parameters  $\boldsymbol{\gamma}[n]$  as follows:

$$\begin{aligned} p(u_c[n]|\gamma_c[n]) &= N(u_c[n]|0, \gamma_c^{-1}[n]) \\ p(\gamma_c[n]) &= Ga(\gamma_c[n]|a_\gamma, b_\gamma), c = 1, \dots, C. \end{aligned} \quad (7)$$

where  $Ga(\cdot|a, b)$  is a gamma PDF with parameters  $a$  and  $b$ . Here we will make  
 use of a popular version of SBL that uses non-informative hyper-prior  $p(\gamma_c[n])$   
 obtained when  $a_\gamma \rightarrow 0$  and  $b_\gamma \rightarrow 0$  [26, 27, 25]. The motivation for this choice  
 210 is twofold. First, the resulting inference schemes typically demonstrate super-  
 ior (or similar) performance as compared to schemes derived based on other  
 hyperprior selections [28]. Second, very efficient inference algorithms can be  
 constructed and studied [29, 30, 31, 32, 33].

The final ingredient is the prior gas concentration  $p(\mathbf{f}[0]).$  Since we have no  
 215 information about the initial gas concentration distribution, we choose  $p(\mathbf{f}[0])$   
 with zero mean and a very high variance:  $p(\mathbf{f}[0]) = \prod_{c=1}^C N(f_c[n]|0, 10^3).$

Now, using Bayes theorem we can construct the desired posterior PDF for  
 the processes of interest by combining (5), (6), (7) and the prior  $p(\mathbf{f}[0])$  as

follows:

$$\begin{aligned}
& p(\mathbf{f}[0] \dots \mathbf{f}[N], \mathbf{u}[1] \dots \mathbf{u}[N], \boldsymbol{\gamma}[1] \dots \boldsymbol{\gamma}[N] | \mathbf{y}[1] \dots \mathbf{y}[N]) = \\
& \mathbf{f}[0] \prod_{n=1}^N p(\mathbf{y}[n] | \mathbf{f}[n]) p(\mathbf{f}[n] | \mathbf{f}[n-1], \mathbf{u}[n]) \\
& \prod_{c=1}^C p(u_c[n] | \gamma_c[n]) \prod_{c=1}^C p(\gamma_c[n]). \tag{8}
\end{aligned}$$

Let us point out that the prior  $p(\mathbf{u}[n], \boldsymbol{\gamma}[n])$  not only reflects the fact that there are only a few “active” cells with sources. Essentially the prior also plays the role of a regularization term in a classical deterministic setting. To be more precise, inspecting the log of a posterior (8) would reveal that the prior (7) introduces a penalty term  $\sum_c \gamma_c[n] (u_c[n])^2$ , which is a weighted  $\ell_2$ -norm of the vector  $\mathbf{u}[n]$ . From a perspective of exploration the regularization is an important part of the observation procedure. In fact, solving equations arising from the FDM for  $\mathbf{u}[n]$  without the regularization would not be possible at early phases of the exploration, since there will be too few measurements available.

### 3.2. Uncertainty Quantification

The key idea of our exploration strategy is to direct robots to regions, where our knowledge about the explored process is currently low. This requires a mechanism for quantifying the information we have about the process itself or process parameters. In particular, in our context if the uncertainty about the gas concentration value or source strength in a grid cell is high, then this grid cell is a good candidate for the next measurement location. To implement this mechanism we intend to make use of the developed probabilistic model.

Indeed, the PDFs of variables associated with a grid cell – gas concentration or source intensity – can be used to compute the amount of information we have about these variables. In order to evaluate only a single grid cell, we calculate the marginal PDF for each cell based on the joint posterior (8). Generally, the marginal results from integrating over all other variables and parameters. Here, this means to calculate  $C$  marginal distribution each time integrating over  $C-1$  variables. While in simple cases like a Gaussian distribution, the marginals

could be calculated in closed form, the introduction of the Gamma distribution in the hierarchical prior prevents an analytical calculation in our case. Yet as we will show, the marginalization can be performed efficiently by representing (8) using a factor graph [34] and performing inference on this graph using message passing algorithms (see also [22]). This algorithm and its implementation is described in more detail in the next section. As a result we obtain the marginal distribution of the source strength  $u_c[n]$  and gas concentration  $f_u[n]$ .

It has been shown in [22] that the marginal distributions of both gas concentration and source intensity in a grid cell can be approximated with Gaussian PDF. As such, the second order moments of these variables can be used as a gauge of the information content<sup>1</sup>. Those second order moments, i.e. the variances, are used to quantify the uncertainty, where cells with a higher variance are more uncertain and interesting location for a new measurement.

#### 4. Distributed Implementation

As described in the previous section, marginals are the foundation of the uncertainty quantification. This chapter explains how to calculate those marginal PDFs in a distributed fashion based on the probabilistic formulation of the posterior (8). In a first step we introduce a graphical representation of our posterior PDF. This graphical representation is used to derive a MP algorithm that calculates the marginals of the required variables in a distributed fashion. Further we show how implemented on our multi-robot system. The used approach is similar to our previous work, for a detailed derivation of the algorithm and equations the reader is referred to [22].

##### 4.1. Factor Graph Representation

For a detailed introduction of Factor Graphs (FGs) we refer the reader to [34]. A FG is an undirected bipartite Bayesian network being composed of

---

<sup>1</sup>Recall that for a Gaussian random variable the entropy is related to the square root of the variable's variance.

value nodes, which represent random variables, and factor nodes, which model functional dependencies between them given by a factorized function. An interesting property of our posterior PDF (8) is the fact that the function is nicely  
 270 factorized. When plugging equation (5) into (8), it can be seen that there are three factors for each cell  $c$  and one factor for each taken measurement. Based on the factorized formulation we can sketch a graphical representation of the posterior. The result is a so called FG [35]. Figure 1 depicts the FG for our posterior PDF (8) for a single cell. The variable nodes (spheres) correspond  
 275 to the random variables of the concentration  $f_c[n]$ , source strength  $u_c[n]$  and hyper-parameter  $\gamma_c[n]$ . Those variables are put into a relation by the factor nodes. The factor nodes model the dependencies and constraints according to the factorized posterior formulation. The factor node  $R_c$  and its connection depend on two aspects: (i) the used PDE (here equation (1)) and (ii) the method  
 280 of the numerical approximation of the PDE. This node puts the concentration values  $f_c$  of the neighboring grid cells into a relation with the source strength  $u_c[n]$  of the cell according to equation (5). The other two factors, the parametric prior  $p(u_c[n]|\gamma_c[n])$  and the hyper-prior  $p(\gamma_c[n])$  of (8) for a cell correspond to the factor nodes  $G_c$  and  $H_c$ . In case a measurement was taken in the considered  
 285 cell, a further factor node  $Y_c$  models the corresponding factor that is related to the likelihood (6). If no measurement is available for the cell this factor node is not present in Figure 1.

#### 4.2. Message Passing Algorithm

Essentially, the FG is the basis for designing a MP algorithm. MP is a powerful tool to calculate marginal distributions given a FG. For our considered problem, the sum product algorithm [36] (also called loopy belief propagation) and variational MP [37] are used. Those algorithms work as follows: Messages are sent between nodes of the FG along the edges. There are two possible types of messages: messages from factor nodes to variable nodes and vice versa. The messages themselves represent beliefs, i.e. also probabilistic distributions. In general the outgoing messages of a node are functions of incoming messages

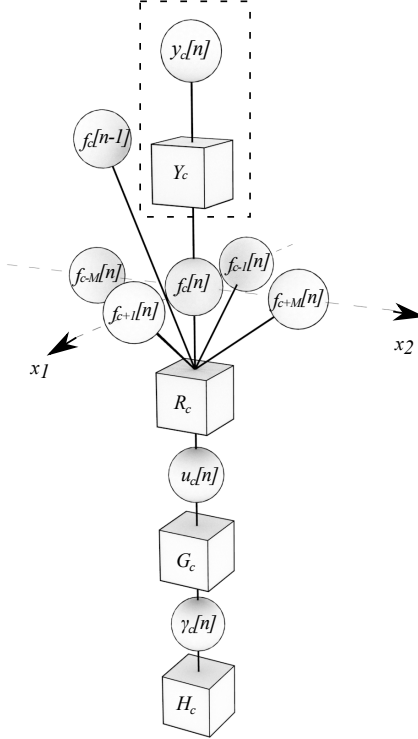


Figure 1: Factor Graph: This graph represents the part of the posterior PDF associated with a single grid cell. It models the relations between variable nodes (spheres) by factor nodes (cubes).

(For the specific calculation rules see [34, 37]). By iteratively exchanging messages between nodes, the outgoing messages of variable nodes converge to the marginal distribution of the corresponding variable or parameter. We make use of the following notation for a message outgoing from node 1 towards node 2:  $m_{node1 \rightarrow node2}$ . In our graph Fig. 1 all messages connected to  $R_c$  and  $Y_c$  could be calculated according to the sum product algorithm. Moreover, the messages – more precisely their probabilistic distributions – are Gaussian distributions:  $m_{node1 \rightarrow node2} = N(x | \mu_{node1 \rightarrow node2}, \tau_{node1 \rightarrow node2}^{-1})$ . Therefore they could be fully specified by their mean  $\mu_{node1 \rightarrow node2}$  and precision  $\tau_{node1 \rightarrow node2}$ , which can be calculated in closed form. Thus, only those two values have to be send

along the edges of the graph. The actual rules for calculating the messages are summarized in Table 1. (For a detailed derivation of the equations please see [22].) In the context of Table 1 we would like to remark that  $\mu_{Y_c \rightarrow f_c[n]}$  corresponds to the actual measured value and  $\mathcal{N}(c)$  denotes the set of all neighbored cells of  $c$  excluding  $c$  itself. Further, we introduce the auxiliary vectors

$$\mathbf{s}_c[n] = [f_c[n], f_{c-1}[n], f_{c+1}[n], f_{c-J}[n], f_{c+J}[n], f_c[n-1]]^T$$

$$\mathbf{z}_c[n] = [f_{c-1}[n], f_{c+1}[n], f_{c-J}[n], f_{c+J}[n], f_c[n-1], u_c[n]]^T.$$

which aggregate all concentrations  $f_{c' \in \mathcal{N}(c)}$  together with  $f_c$  and the source strength  $u_c$ , receptively.  
290

Message	Equation
$m_{Y_c \rightarrow f_c[n]}$	$N(f   \mu_{Y_c \rightarrow f_c[n]}, \tau_m^{-1})$
$m_{f_c[n] \rightarrow R_c}$	$m_{Y_c \rightarrow f_c[n]} \prod_{c' \in \mathcal{N}(c)} m_{R_{c'} \rightarrow f_c[n]}$
$m_{R_c \rightarrow u_c[n]}$	$\int e^{-\frac{\tau_s}{2} (r_c(\dots))^2} \times m_{f_c[n-1] \rightarrow R_c} \times m_{f_c[n] \rightarrow R_c} \times$ $\times \prod_{c' \in \mathcal{N}(c)} m_{f_{c'}[n] \rightarrow R'_c} d\mathbf{s}_c[n]$
$m_{R_c \rightarrow f_c[n]}$	$\int e^{-\frac{\tau_s}{2} (r_c(\dots))^2} \times m_{f_c[n-1] \rightarrow R_c} \times m_{u_c[n] \rightarrow R_c} \times$ $\times \prod_{c' \in \mathcal{N}(c)} m_{f_{c'}[n] \rightarrow R_c} d\mathbf{z}_c[n]$
$m_{u_c[n] \rightarrow R_c}$	$\begin{cases} N(u_c   \frac{\mu_c^2 \tau_c - 1}{\mu_c \tau_c}, (\tau_c + \frac{\tau_c}{\tau_c \mu_c^2 - 1})^{-1}); & \tau_c \mu_c^2 - 1 > 0 \\ N(u_c   0, \infty^{-1}) = \delta(u_c); & \tau_c \mu_c^2 - 1 \leq 0. \end{cases}$ <p>with <math>\mu_c = \mu_{R_c \rightarrow u_c[n]}</math> and <math>\tau_c = \tau_{R_c \rightarrow u_c[n]}</math></p>

Table 1: Update rules for the message passing algorithm (see [22] for more details)

Messages related to our hierarchical prior and therefore connected to nodes  $G_c$  and  $H_c$  are not analytical tractable by the sum-product algorithm. However,

Variational Message Passing (VMP) provide analytical approximation techniques to calculate these messages. Moreover, as explained in [22] we calculated a fixed point of the messages passing iterations for the messages related to VMP.  
295 Combining this with the other parts of the FG results in the simple update rule for  $m_{u_c[n] \rightarrow R_c}$  summarized in Table 1.

We would like to stress that the FG in Fig. 1 represents only a single cell. The overall graph requires computing the messages for all cells and factors.  
300 Nonetheless, those messages could be calculated in closed form and in random order or all at once in parallel. This makes the algorithm particularly suitable for a distributed implementation on a multi-agent system. To this end, we split the overall graph into different parts that correspond to different 2D regions of our environment. A simplified version of the overall FG and the partitioning  
305 of this graph are exemplarily shown in Fig. 2. For the sake of clarity, the connection to nodes of the previous time stamp are not displayed. Further, the nodes  $Y_c$  are only exemplarily shown for some cells, where it is assumed that a measurement was taken. Each region (i.e. sub-graph) is assigned to one robot of our multi-agent system and each robot is able to calculate all messages  
310 related to its own part. The edges crossing the border of a region are marked as red lines in Fig. 2. Only the messages related to those edges have to be actually exchanged between the agents. After convergence of the algorithm, the variances of the PDFs of  $u_c[n]$  are used to quantify the uncertainty of the corresponding cells (see section 3.2). Based on the uncertainty, each robot can  
315 propose a certain number of cells of interest for the region it is responsible for. Those cells or points of interest are send to all other robots.

## 5. Exploration Procedure

Our exploration strategy utilizes the uncertainty quantification of the estimated source strength for each cell  $c \in C$  with  $C$  being the set of all cells in our environment. For this purpose the cells are rated according to the inverse variance, i.e. precision  $\tau_c[n]$  of the source strength marginal  $p(u_c[n]) \propto$

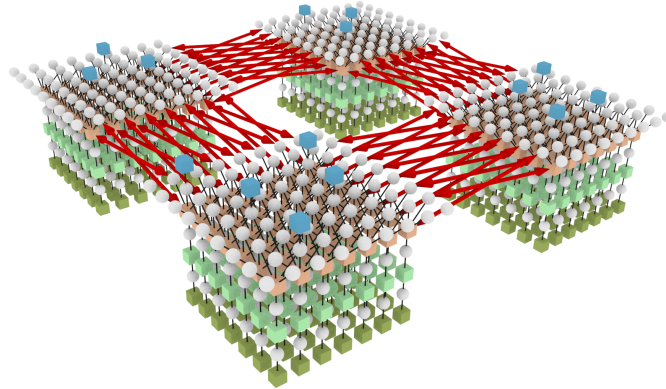


Figure 2: Distributed Factor Graph: This figure illustrates the overall factor graph. This is a simplified version without time dependencies. The graph is spatially split into four regions, where the big arrows represent messages sent between different regions.

$N(\hat{u}_c[n], \tau_c[n])$ . A set  $P$  of cells with the lowest precisions, or, equivalently, with the highest uncertainties, serves as a proposal for new way points for the robots. This is constructed as follows. Each robot  $a$  proposes  $K$  cells from the region  $C_a \subseteq C$  of the environment it is responsible for:

$$\tau_{c_1} \leq \tau_{c_2} \leq \dots \leq \tau_{c_K} \leq \tau_{c_{(K+1)}} \leq \dots; \tau_{c_i} \in C_a$$

The  $K$  cells are then selected and an agent's proposal set  $P_a$  is generated as  $P_a = \bigcup_{i=1}^K \{c_i\}$ . These are then combined to a global set  $P = \bigcup P_a$  for the whole environment. It is from this set  $P$  that way points for individual robots are selected. We would like to emphasize that the movements of a robot are thus not restricted to the region it is responsible for computations due to the distribution MP scheme. In other words, the robot can choose from the whole set  $P$  and therefore move through the whole exploration domain. Clearly, already selected points are removed from  $P$  to avoid conflicts; it is therefore necessary to communicate decisions to all other robots in a swarm.

After the decision is made, a robot moves to the selected way point. To avoid collisions with other robots, we implemented a reactive collision avoidance mechanism. On its way, the robot monitors the current distance to all other

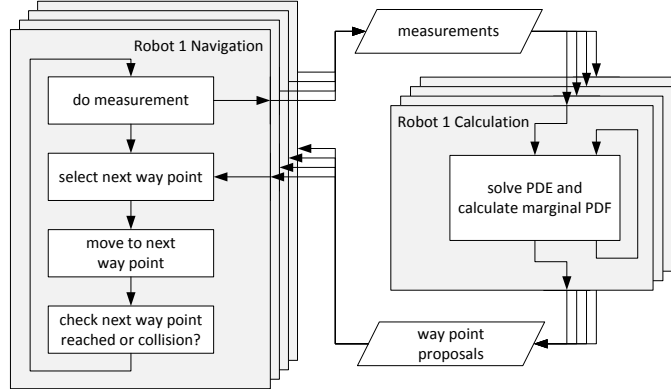


Figure 3: Exploration Procedure: The exploration is implemented with two main loops. The right loop solves the PDE and produces new way point proposals, the left one controls the individual robots.

<sup>330</sup> robots based on received position information. If the distance drops below a defined safety threshold, i.e if two robots getting too close, the robots stop and select another way point from the proposals that would increase the critical distance. Finally, when a robot reaches its goal, it takes a measurement which is incorporated in the approximate, probabilistic inverse solution of the PDE.

<sup>335</sup> The overall procedure is depicted in Fig. 3. As it can be seen, the robotic navigation and solution of the PDE are actually two separate loops. The loops are connected by the data exchange of proposed way points and measurements. We would like to stress that in this way the navigation part of each robot could be realized in an asynchronous fashion, where no robot has to wait for results <sup>340</sup> of the others robots.

## 6. Experimental Setup

In general, it is quite hard to evaluate gas mapping or gas source localization strategies in realistic real-world scenarios. While ground truth data may be available for the source locations, this is not the case for the gas concentration distribution. Even though in this work we mainly focus on the gas source local-

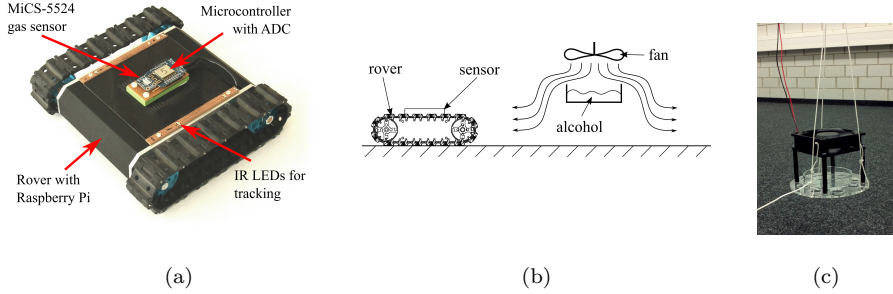


Figure 4: Experimental setup: Picture (a) depicts the robotic platform carrying the gas sensor. The schematic in (b) shows the design of the artificial gas source and (c) a picture of the actual realization.

ization, for better understanding of the used approach an accurate estimation of the gas concentration is also of interest. To address these issues we therefore analyze our exploration strategy in two different types of experiments. First we carry out hardware-in-the-loop experiments with synthetic gas dispersion.  
 350 This implies that a real robotic system is used, yet the gas dispersion process is simulated. In this way we obtain ground truth data of the source distribution and gas concentration from the simulation. However, the simulation uses the same mathematical model as the model-based exploration strategy. This perfect model match is not usually observed in reality. For this reason, we also carry  
 355 out an experiment with a real gas, more specifically with an ethanol vapor, and a robotic swarm in lab conditions.

For our experiments, we developed a small robot. Its main part is a Raspberry Pi 2 – a low power single-board computer with Linux OS (900MHz quad-core ARM Cortex-A7 CPU, 1GB RAM). From this computer it is possible to send  
 360 velocity commands to a micro-controller that implements a velocity controller for two motors driving the tracks of the robot (see picture in Fig. 4a). The experiments were done in a laboratory with a commercial optical tracking system. This system is able to track active infrared LEDs mounted on the robot. It then provides the actual position and orientation of each of the robots with an accuracy of  $\approx 1\text{cm}$ . This can be considered as an almost perfect localization  
 365

with respect to the discretization of the environment with a cell size larger than 10cm. From 3 to 5 robots are used in the experiments. Their computers are connected to an 802.11 wireless LAN communication system. Through this wireless link the robots receive their positioning data and are also able to  
370 exchange messages between themselves. For the software implementation and the inter-process communication we make use of the Robot Operating System (ROS) <sup>2</sup>.

In the hardware-in-the-loop experiments, the gas diffusion is simulated for a two dimensional case. The data are generated according to equation (1). Whenever a measurement is demanded by the exploration procedure for one robot,  
375 this equation is evaluated at the current position of the robot. Additionally, we disturb the measurement by additive white noise  $\xi$ . For the evaluation of the PDE a Finite Volume Method solver [38] is used. For our example scenario, we have chosen a Dirichlet boundary condition  $f(x, t) = 0$ , except for the right border, where we use a Neumann boundary condition  $\frac{\partial f(x, t)}{\partial x} = 0$ . This would  
380 correspond to an open field scenario, where material can flow off at all borders except for the right one because of e.g. a wall. Further, this setting will not reach a steady state. Thus, we can be sure to observe a dynamic process. For the virtual gas simulation we considered the concentration and source strength unit-less. The discrete grid size, the time difference between two discrete time stamps and the diffusion coefficient  $\kappa$  are set to 1 in the simulation. However,  
385 later on the concentration field is fitted to our laboratory with a scale of 6m times 2.4m. Further, the total grid contains  $12 \times 30$  cells.

For the second experiment with the ethanol gas, the rovers are equipped with a MiCS 5524 metal oxide gas sensor (SGX SensorTech Ltd, Switzerland). The sensor voltage is measured with an AD-converter of an ESP8266 microcontroller, which provides the sensor reading to the whole system via wireless LAN. In order to convert the binary values of the ADC to concentrations, we used the data sheet of the sensor [39], which specifies a linear dependency in the

---

<sup>2</sup><http://www.ros.org/>

log-log domain between the sensors resistor  $R_s$  and the ethanol concentration. Therefore, we model this dependency by an exponential function [40]:

$$y = \beta \cdot R_s^\alpha, \quad (9)$$

where  $y$  is the measured gas concentration plugged into our Bayesian approach (i.e.  $y = \mu_{Y_c \rightarrow f_c[n]}$ ). The parameter  $\alpha$  corresponds to the slope of the sensor sensitivity in the log-log domain. According to the data sheet it is set to  $\alpha = -1.6$ . The parameter  $\beta$  was chosen in a way that  $y$  is unit-less and roughly in the range of  $[0, 1]$ ). In this way, we can use the exact same parametrization of the algorithm as in the hardware-in-the-loop case, where we considered unit-less concentration and source values in the same range. Further, the parameter  $\beta$  is individually adjusted for each sensor so that the sensor response is the same for all sensors when all of them were exposed to the same constant concentration. In our case  $\beta$  was chosen in the order of 10. The resistor  $R_s$  was calculated according to the measured voltage drop  $U$  on a load resistance  $R_L$  of a voltage divider consisting of  $R_s$  and  $R_L$  as follows:

$$R_s = R_L (5V/U - 1) \propto (5V/U - 1). \quad (10)$$

We would like to remark that we incorporate  $R_L$  in the constant  $\beta$  when inserting (10) into (9).

As an artificial gas source in the experiments we used ethanol evaporating from a culture dish (80mm diameter) filled with approximately 5g of 94% ethanol assay. Above the culture dish we mounted a small fan (see Fig. 4c). The airflow caused by this fan avoids a saturation of ethanol concentration in the layer above the liquid. Thus, it accelerates the evaporation. Moreover, the air flow facilitates a radial dispersion of the ethanol gas. The whole structure hangs down from the ceiling, so that the rovers are able to drive below the source without any collision.



Figure 5: Lab Environment: The picture shows our lab during an experiment. The simulated concentration field is projected to the ground in a post-processing step. A video of an experiment can be found here: <https://youtu.be/UJYwdzrDTL4>.

## 7. Evaluation

400 In this section the results of our experimental studies are presented. First, we show the performance of the proposed exploration strategy for the hardware-in-the-loop experiment. Then, the second experiment with a real ethanol gas dispersion is discussed.

### 7.1. Hardware-in-the-loop exploration experiment

405 To evaluate the performance, we compared the proposed exploration strategy against exploration with a predefined sweeping trajectory. The sweeping trajectories are generated by dividing the environment into five equal regions and generating a predefined “meander” trajectory for each of these regions. In this way the measurements will fully cover the whole environment after a certain time, i.e. each grid cell is measured at least once. This strategy is reasonable  
410 if no prior knowledge or model assumptions are available. We compare the performance of the strategies by means of efficiency (in terms of the required number of measurement samples needed to achieve convergence of the source signals) and quality of the estimates in terms of the achievable estimation error.

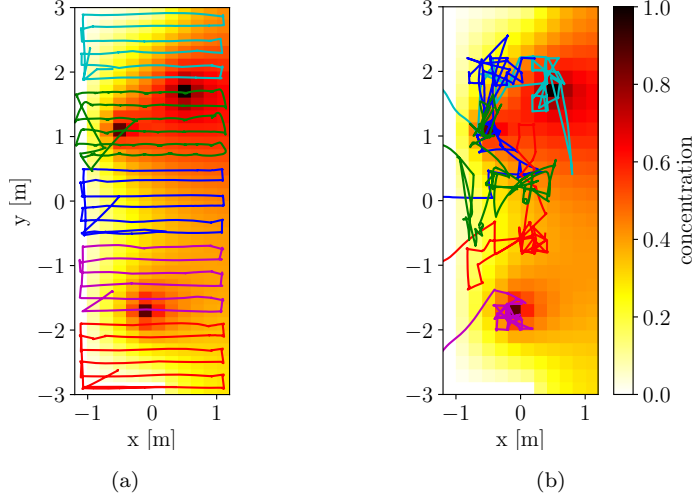


Figure 6: Hardware-in-the-loop experiments: The figure compares the meander trajectory (a) and the proposed exploration strategy (b). The trajectories superimpose the simulated concentration field.

415 Note that using the number of measurement instead of using the actual time  
 for the exploration is of an advantage in our case, since the actual time highly  
 depends on the time spent on making a measurement; these are different for  
 hardware-in-the-loop and real gas measurements. Also, in order to see how well  
 the spatially distributed sources  $\mathbf{u}[n]$  are identified, we use a so-called Earth  
 420 Mover's Distance (EMD) measure, which is an analog of a Wasserstein metric  
 for discrete distributions [41]. EMD measures the effort needed to "displace" one  
 distribution onto another one; it is thus particularly useful for comparing sparse  
 functions. Specifically, we compare the estimated vector  $\mathbf{u}[n]$  with the ground  
 truth vector  $\hat{\mathbf{u}}$  with all elements set to zero except for the three cells containing  
 425 a source ( $\hat{u}_c = 1.0$  at  $x = -0.2m, y = -1.8m$ ;  $\hat{u}_c = 1.0$  at  $x = -0.6m, y = 1.0m$ ;  
 $\hat{u}_c = 0.8$  at  $x = 0.4m, y = 1.6m$ ). Besides, we use the Normalized Mean Square  
 Error (NMSE) ( $= \|\mathbf{f}[n] - \hat{\mathbf{f}}[n]\|^2 / \|\hat{\mathbf{f}}[n]\|^2$ ) to quantify the concentration esti-  
 mation error. This is possible, since ground truth data  $\hat{\mathbf{f}}[n]$  are available from

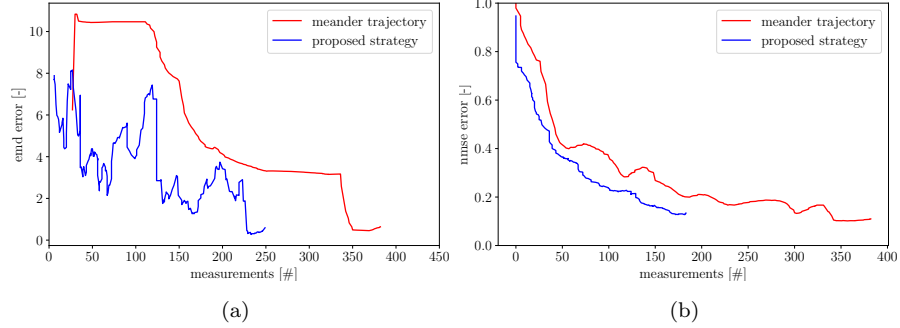


Figure 7: Hardware-in-the-loop results: The two plots compare the performance of the meander trajectory and the proposed exploration strategy. In (a) the error is plotted measured regarding the estimated source distributions by means of the Earth Mover’s Distance (EMD). In (b) the Normalized Mean Square Error (NMSE) of the estimated concentration field compared to the ground truth is shown.

the simulated gas diffusion process. The corresponding results are shown in Fig. 6 and Fig. 7 for the considered experiment.

Fig. 6a and Fig. 6b present the trajectories of the meander and the proposed exploration strategy. Let us re-iterate that the very nature of the proposed exploration strategy is adaptive, i.e., the algorithm will react to the made measurements. As such, the trajectory is not deterministic . The generated trajectories are overlaid with the simulated concentration field computed at the time when the sources were correctly identified. It can be seen that the gas distribution is driven by three sources located at the concentration peaks.

Fig. 7 depicts the estimation performance for both source and concentration signals for the compared exploration strategies. The curves in Fig. 7a show the EMD error between the estimated source distribution  $\hat{u}[n]$  and the true source distribution  $u$  in relation to the number of collected measurements. The curves in Fig. 7b depict the NMSE between the estimated concentration field and the ground truth. As we see, using the meander trajectory the multi-agent system is able to identify the source distribution after approximately 340 measurements. This indicates the step in the convergence curve towards zero in Fig. 7a. In

general, the performance of the meander highly depends on the position of the sources. If they are already covered at the beginning of the trajectory, of course fewer measurements are needed. However, to be conservative the worst case has to be considered and this means a full coverage of the region. In our  
450 example, 360 measurements would be necessary for that. In contrast, the curve for the proposed exploration strategy converges with only 230 measurements in Fig. 7a. This indicates that robots were able to identify the sources with fewer measurements. As can be seen from the trajectory in Fig. 6b the measurements are concentrated around the source locations. Obviously, the corresponding  
455 measurements contain more information about the sources. This is the reason for a better performance of the proposed exploration strategy. Based on Fig. 7b, it can be seen that the estimated concentration field for both strategies reaches a low NMSE. Here the performance of the proposed strategy is better, too, however subjectively speaking the difference is small according to Fig. 7b.

460 Additionally, the hardware-in-the-loop experiments enable us to analyze other performance indicators of our algorithm and system properties. For example we can measure the gross data rates containing all overheads caused by ROS, OS, TCP etc. Specifically, in our case a data rate of less than 70kBytes/s  
465 is required for the communication link between two robots. This allows us to define specifications for a communication system required for future real-world experiments. Similarly, we can investigate the processor load of the on-board computers caused by the algorithm. In particular, the on-board computers were able to generate way point proposals with an update-rate of 1.0Hz. This is fast enough for typical application, especially if you consider the measuring and  
470 recovering time of typical MOX sensors.

## 7.2. Real Gas Experiment

Now, we consider the experiment with a real ethanol gas dispersion. In a first step we repeated the exploration with a predefined sweeping trajectory. In this experiment the ethanol source as described in section 6 was placed in the middle  
475 of our  $3 \times 6\text{m}$  lab environment. The environment was discretized by  $15 \times 30$  grid

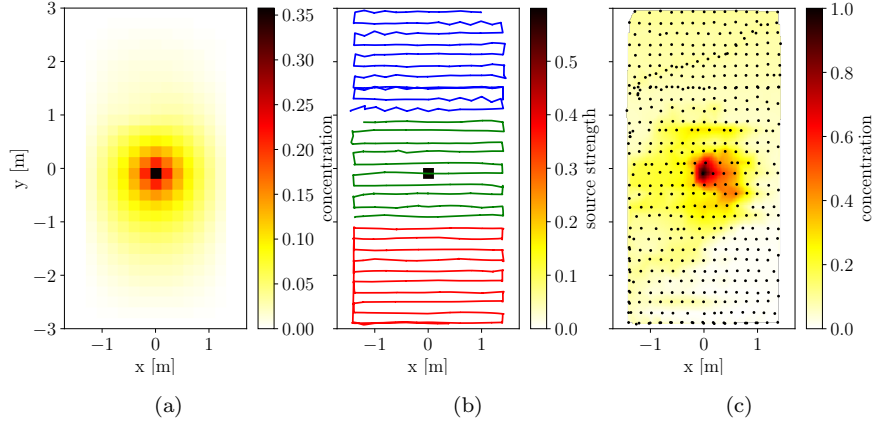


Figure 8: Meander trajectory: The figure shows the results of sampling the real ethanol gas distribution by means of a meander trajectory. Where (a) depicts the estimated gas distribution based on the PDE model and (b) respectively the estimated source distribution where a single peak in  $x=0$ ,  $y=0$  has been detected, plot (c) illustrates the raw measurements taken at the location marked by a dot and linearly interpolated in between. Additionally, the trajectories of the rovers are shown in (b).

cells. In the experiment we assume Dirichlet boundary condition  $f(x, t) = 0$  at the borders of the exploration environment. Note that this assumption is only chosen due to a lack of the actual knowledge about the conditions at the border and also causes a mismatch between the reality and the used model. To explore the gas distribution and to find the source three rovers are used. Also, in order to take the inertia of the gas sensor into account (response time of the sensor is < 2s [42]) a specific measurement procedure is designed as follows:

1. once the rover arrives to the target position, it stops
2. it then waits for 1s to allow the sensor to reach a steady state.
- 485 3. afterwards, a measurement starts over the time period of 5s
4. finally, the robot moves to the next measurement position.

Thus, the actual measurement at one position is average over 5s. Such a long measurement time is needed to reduce the measurement noise caused by the

ADC, or short time-scale turbulence in the airflow. However, as the performance  
490 is measured with respect to the number of measurements, the actual time needed  
to take a measurement plays a minor role in the evaluation of the results.

The results of this meander exploration are shown in Fig 8. In Fig 8b the  
trajectories are plotted as an overlay above the estimated source distribution,  
while Fig 8a shows the estimated gas concentration based on the PDE model.  
495 Here the source distribution corresponds to a single peak (back square) at  $x =$   
 $0, y = 0$ . Further, Fig 8c depicts the raw concentration measurements collected  
at the locations marked with a dot.<sup>3</sup>

As can be seen, the model-based estimated gas concentration in Fig 8a differs  
from the raw observations in Fig 8c. Although the estimated gas distribution  
500 exhibits a nice radial shape, the real concentration shows an asymmetric pattern.  
This asymmetric pattern with increased concentration in the lower left area was  
observed during multiple sweeping experiments. A possible explanation for this  
phenomenon would be a room specific airflow, caused by a none-airtight door  
505 located in the lower left corner of the lab, or by an aligned temperature-gradient  
in the room. Even though, the observations of the real gas dispersion do not  
perfectly match with our model assumption, the source position estimated based  
on the model is correct within the accuracy of the discretization. Thus, the  
diffusion PDE sufficiently approximates the real gas dispersion in the scenario  
considered here. It shows the advantage of the probabilistic approach that is  
510 able to deal with imperfect model assumptions.

As we can see from the experiments with a meander-based movement strat-  
egy, having a sufficient number of measurements allows a PDE-based diffusion  
model to approximate well the gas and source distribution. Now, in the second  
step we switch to the proposed model-based exploration strategy as described  
515 in Section 5. We also keep the same experimental setup. The corresponding  
results are shown in Fig. 9. This experiment was carried out 30min after the

---

<sup>3</sup>Between the measurement locations the concentration was linearly interpolated to better  
visualize the raw data.

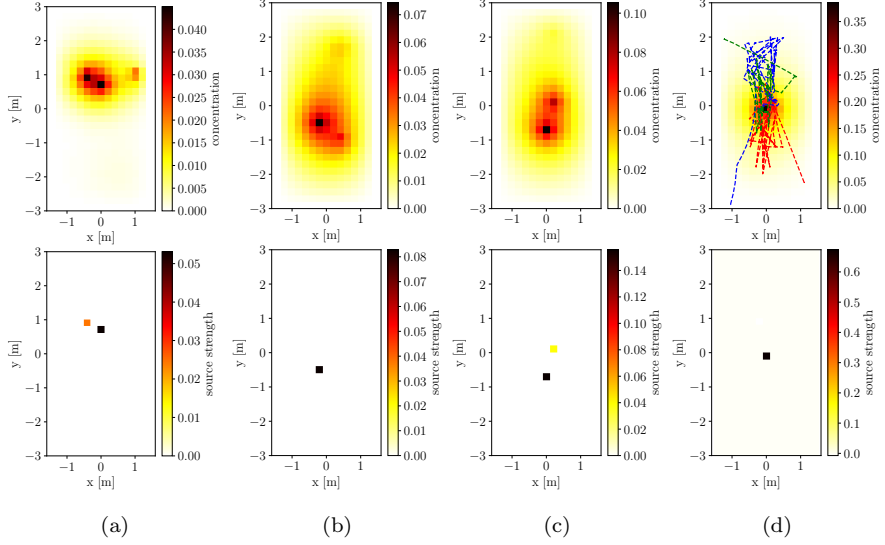


Figure 9: Proposed strategy: Here four snapshots of the estimated concentration and source distribution are shown. In (a) after 30s and 6 measurements, in (b) after 120s and 30 measurements, in (c) after 200s and 53 measurements and in (d) after 230s and 62 measurements. The trajectories of the three robots are shown in (d).

meander experiment. In Fig. 9a to 9d snapshots of the estimated concentration and source distribution are shown.

In Fig. 10 we compare the performance of the meander trajectory with that generated by the proposed exploration strategy using the same EMD and NMSE metrics as in first experiment. Let us also point out that for some time instances the estimated source distribution was equal exactly zero all grid cells. For these cases the EMD criterion could not be computed. Thus, we excluded these occurrences from the performance plot in 10a and linearly interpolated the error curve; these segments are indicated by dotted lines. Considering that the grid contains 450 cells and the source is located exactly in the middle of the second meander trajectory (i.e. green in Fig. 8b), it is no surprise that the source is correctly identified after approximately 225 measurements by the meander trajectory. In contrast by the proposed strategy the rovers were able to identify the source after approximately 60 measurements. At this point we would like

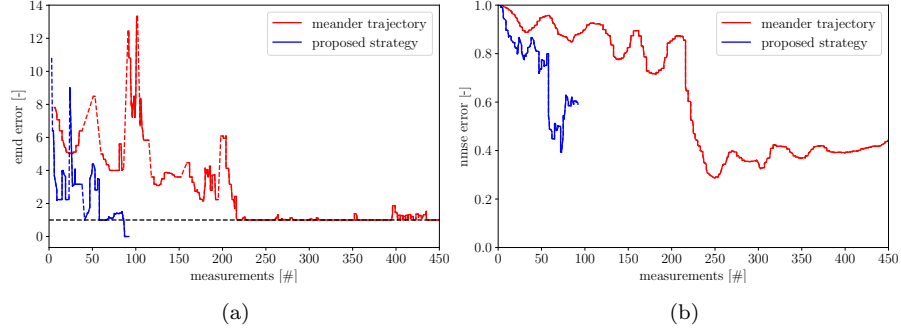


Figure 10: Performance in real experiments: The two plots compare the performance of the meander trajectory and the proposed exploration strategy. In (a) the error is plotted measured regarding the estimated source distributions by means of the Earth Mover’s Distance (EMD). Here ground truth data were available. The plot (b) shows the Normalized Mean Square Error (NMSE) of the estimated concentration field compared to the raw data collected by the meander in Fig 8c.

to comment on the discretization that was used. Based on that, here a perfect localization within the accuracy of the discretization corresponds to an EMD of equal or less than 1. This is due to the fact that in our setup the actual source is located at the edge of two cells, but for calculating the EMD we considered the ground truth source distribution as a single peak located only in one cell.  
535

In contrast to the hardware-in-the-loop experiments, in the real world experiments the NMSE in Fig.10b of the estimated concentration is rather high. Of course, this is not a very precise indicator, since the concentration was not compared to real ground truth values but to the collected raw data by the meander trajectory. However, it gives a first hint on a certain mismatch between  
540 the model assumptions of the gas dispersion and reality. Besides, the meander strategy finally achieves a lower NMSE in Fig.10b compared to the proposed strategy. This shows that while the proposed strategy is better for source localization, for concentration mapping tasks a predefined sweeping trajectory may be better.  
545

## 8. Discussion and Conclusion

The results of the experiments have shown that a model-based exploration is of advantage for sampling a gas diffusion process in order to localize gas sources. By an intelligent exploration strategy, the number of required measurements can  
550 be reduced while the capability to locate gas sources (and to some degree also to gas distributions) is preserved. This property is favorable for applications, where a measurement is expensive or consumes a lot of time.

The potential of the presented approaches arises from the uncertainty driven strategy for taking new measurements in combination with the assumption that  
555 the sources are sparsely distributed in the environment and their number is small. This assumption is encoded with a prior PDF that assumes the probabilistic source strength distribution to have zero mean and unknown variance. Under this assumption evidence for a source with non-zero posterior mean effectively “contradicts” this prior assumption; as such the uncertainties of the estimated sources in the corresponding regions grow. As a consequence, the robots  
560 concentrate their measurements on informative regions around the sources according to the proposed exploration strategy. Additionally, this implies a need to employ a multi-robot system with more agents than gas sources, since single robots may get stuck in the neighborhood of a source and thus cannot discover new sources. Multiple rovers, however, are able to effectively reduce the uncertainty around the sources by multiple simultaneous measurements, and individual robots can ”escape” from the source location. In future work a mechanism  
565 to declare a source as being found, after its PDF has converged, may also help to explore other regions not visited yet.

In the hardware-in-the-loop experiments we have shown the potential of this  
570 model-based multi-robot exploration for gas source localization. While it seems obvious that prior information based on a model facilitates the exploration, it is unclear how the model-mismatch between the used dispersion model and real gas dispersion affects the exploration. In the experiments with ethanol  
575 gas we have shown that our exploration approach is able to handle some of

model-mismatches quite well. A key reason for the mismatch are turbulence and advection mechanisms that are not explicitly represented with model (1), but are important phenomena in reality. How to incorporate those effects into the model is part of future work. For example, the advection-based diffusion  
580 can be incorporated directly into the PDE through a convection term.

A further important advantage of the presented approach is its robustness with respect to the sensor calibration. Correct concentration measurements with exact scaling are not needed. Instead normalized concentration values are sufficient as long as the outputs of the sensors on different robots are all in  
585 the same range. Moreover, we noticed that it is even possible to localize the source when a linear relation between the concentration and the sensor voltage is assumed.

Nonetheless, there are also some limitations of the presented approach. For instance in the experiments the source was placed in the middle of the region  
590 to be explored. In general is it easier to locate a source that is farther away from the border. Furthermore, only one source was considered in the real world experiments. Thus, additional experimental studies should be considered in future work.

In summary, let us mention that realistic gas dispersion problems are complex dynamical processes. From a practical perspective having a very complex  
595 model that adequately represents reality might lead to computationally very complex inverse problems. Instead, simpler probabilistic models, like the one used in this work, can be seen as a numerically feasible approximation, which can be estimated based on concentration measurements in an adequate (in the  
600 context of robotic exploration) amount of time.

## Acknowledgment

This work has partly been supported within H2020-ICT by the European Commission under grant agreement number 645101 (SmokeBot).

## References

- [1] A. Marjovi, L. Marques, Multi-robot odor distribution mapping in realistic time-variant conditions, 2014 IEEE International Conference on Robotics and Automation (ICRA) (2014) 3720–3727doi:10.1109/ICRA.2014.6907398.
- [2] A. J. Lilienthal, A. Loutfi, T. Duckett, Airborne chemical sensing with mobile robots, Sensors 6 (11) (2006) 1616–1678. doi:10.3390/s6111616. URL <http://www.mdpi.com/1424-8220/6/11/1616>
- [3] G. Kowadlo, R. A. Russell, Robot odor localization: A taxonomy and survey, International Journal of Robotics Research 27 (8) (2008) 869–894. doi:10.1177/0278364908095118.
- [4] H. Ishida, Y. Wada, H. Matsukura, Chemical sensing in robotic applications: A review, IEEE Sensors Journal 12 (11) (2012) 3163–3173. doi:10.1109/JSEN.2012.2208740.
- [5] A. Lilienthal, T. Duckett, Building gas concentration gridmaps with a mobile robot, Robotics and Autonomous Systems 48 (1) (2004) 3–16. doi:10.1016/j.robot.2004.05.002.
- [6] R. A. Russell, A. Bab-Hadiashar, R. L. Shepherd, G. G. Wallace, A comparison of reactive robot chemotaxis algorithms, Robotics and Autonomous Systems 45 (2) (2003) 83–97. doi:10.1016/S0921-8890(03)00120-9.
- [7] B. Gao, H. Li, F. Sun, 3D moth-inspired chemical plume tracking, 2015 IEEE International Conference on Robotics and Biomimetics, IEEE-ROBIO 2015 24 (1) (2015) 1786–1791. doi:10.1109/ROBIO.2015.7419031.
- [8] H. Hajieghrary, M. A. Hsieh, I. B. Schwartz, Multi-agent search for source localization in a turbulent medium, Physics Letters, Section A: General, Atomic and Solid State Physics 380 (20) (2016) 1698–1705. doi:10.1016/

j.physleta.2016.03.013.

URL <http://dx.doi.org/10.1016/j.physleta.2016.03.013>

- [9] M. Vergassola, E. Villermaux, B. I. Shraiman, 'Infotaxis' as a strategy for searching without gradients, *Nature* 445 (7126) (2007) 406–409. arXiv: 635 t8jd4qr3m, doi:10.1038/nature05464.
- [10] H. Ishida, Y. Kagawa, T. Nakamoto, T. Moriizumi, Odor-source Localization In Clean Room By Autonomous Mobile Sensing System, Proceedings of the International Solid-State Sensors and Actuators Conference - TRANSDUCERS '95 1 (1995) 115–121. doi:10.1109/SENSOR.1995.640 717349.
- [11] J. G. Monroy, J.-L. Blanco, J. Gonzalez-Jimenez, Time-variant gas distribution mapping with obstacle information, *Auton. Robots* 40 (1) (2016) 1–16. doi:10.1007/s10514-015-9437-0.
- [12] S. Li, Y. Guo, B. Bingham, Multi-robot cooperative control for monitoring and tracking dynamic plumes, Proceedings - IEEE International Conference on Robotics and Automation (2014) 67–73doi:10.1109/ICRA.2014.645 6906591.
- [13] M. A. Demetriou, T. Egorova, N. A. Gatsonis, Estimation of a gaseous release into the atmosphere using a formation of UAVs, IFAC-PapersOnLine 650 49 (18) (2016) 110–115. doi:10.1016/j.ifacol.2016.10.148.  
URL <http://dx.doi.org/10.1016/j.ifacol.2016.10.148>
- [14] M. A. Demetriou, D. Ucinski, State Estimation of Spatially Distributed Processes Using Mobile Sensing Agents, American Control Conference (ACC) (2011) 1770–1776.
- [15] F. Pukelsheim, Optimal Design of Experiments, John Wiley & Sons, Inc., 655 1993.
- [16] D. Uciński, Optimal Measurement Methods for Distributed Parameter System Identification, CRC Press, 2004.

- [17] A. J. Lilienthal, M. Reggente, M. Trincavelli, J. L. Blanco, J. Gonzalez,  
660       A statistical approach to gas distribution modelling with mobile robots-the kernel dm+ v algorithm, Intelligent Robots and Systems, 2009. IROS 2009. IEEE/RSJ International Conference on (2009) 570–576doi:10.1109/IROS.2009.5354304.
- [18] J. G. Monroy, A. J. Lilienthal, J. L. Blanco, J. Gonzalez-Jimenez, M. Trincavelli, Probabilistic gas quantification with MOX sensors in Open Sampling Systems - A Gaussian Process approach, Sensors and Actuators, B: Chemical 188 (2013) 298–312. doi:10.1016/j.snb.2013.06.053.  
665       URL <http://dx.doi.org/10.1016/j.snb.2013.06.053>
- [19] D. J. C. MacKay, Information-Based Objective Functions for Active Data Selection, Neural Computation 4 (4) (1992) 590–604. doi:10.1162/neco.1992.4.4.590.  
670
- [20] P. Whaite, F. Ferrie, Autonomous exploration: driven by uncertainty, IEEE Transactions on Pattern Analysis and Machine Intelligence 19 (3) (1997) 193–205. doi:10.1109/34.584097.
- [21] T. Wiedemann, C. Manss, D. Shutin, A. J. Lilienthal, V. Karolj, A. Viseras,  
675       Probabilistic modeling of gas diffusion with partial differential equations for multi-robot exploration and gas source localization, in: 2017 European Conference on Mobile Robots (ECMR), 2017, pp. 1–7. doi:10.1109/ECMR.2017.8098707.
- [22] T. Wiedemann, C. Manss, D. Shutin, Multi-agent exploration of spatial dynamical processes under sparsity constraints, Autonomous Agents and Multi-Agent Systems 32 (1) (2018) 134–162. doi:10.1007/s10458-017-9375-7.  
680       URL <https://doi.org/10.1007/s10458-017-9375-7>
- [23] J. C. Strikwerda, Finite Difference Schemes and Partial Differential Equations, 2nd Edition, Society for Industrial and Applied Mathematics, Philadelphia, 2004.  
685

- [24] W. Gong, Approximations of Parabolic Equations With Measure Data, MATHEMATICS OF COMPUTATION 82 (281) (2013) 69–98. doi:10.1090/S0025-5718-2012-02630-5.
- [25] M. E. Tipping, Sparse Bayesian Learning and the Relevance Vector Machine, Journal of Machine Learning Research.
- [26] D. Wipf, S. Nagarajan, A New View of Automatic Relevance Determination, Advances in Neural Information Processing Systems 20 (2008) 1625–1632.
- [27] D. P. Wipf, B. D. Rao, Sparse Bayesian learning for basis selection, Signal Processing, IEEE Transactions on 52 (8) (2004) 2153–2164. doi:10.1109/TSP.2004.831016.
- [28] R. Giri, B. Rao, Type i and type ii bayesian methods for sparse signal recovery using scale mixtures, IEEE Transactions on Signal Processing 64 (13) (2016) 3418–3428. doi:10.1109/TSP.2016.2546231.
- [29] M. E. Tipping, A. Faul, J. J. T. Avenue, J. J. T. Avenue, Fast marginal likelihood maximisation for sparse bayesian models, in: Proceedings of the Ninth International Workshop on Artificial Intelligence and Statistics, 2003, pp. 3–6.
- [30] D. Shutin, T. Buchgraber, S. R. Kulkarni, H. V. Poor, Fast variational sparse bayesian learning with automatic relevance determination for superimposed signals, IEEE Transactions on Signal Processing 59 (12) (2011) 6257–6261. doi:10.1109/TSP.2011.2168217.
- [31] D. Shutin, S. R. Kulkarni, H. V. Poor, Incremental reformulated automatic relevance determination, IEEE Transactions on Signal Processing 60 (9) (2012) 4977–4981. doi:10.1109/TSP.2012.2200478.
- [32] D. Wipf, S. Nagarajan, A new view of automatic relevance determination, in: Proceedings of the 20th International Conference on Neural Information Processing Systems, NIPS'07, Curran Associates Inc., USA, 2007, pp.

- 1625–1632.
- URL <http://dl.acm.org/citation.cfm?id=2981562.2981766>
- [33] T. L. Hansen, B. H. Fleury, B. D. Rao, Superfast Line Spectral Estimation, ArXiv e-printsarXiv:1705.06073.
- [34] H. A. Loeliger, An Introduction to Factor Graphs, *Signal Processing Magazine*, IEEE 21 (1) (2004) 28 – 41.
- [35] F. R. Kschischang, B. J. Frey, H. Loeliger, Factor graphs and the sum-product algorithm, *IEEE Transactions on Information Theory* 47 (2) (2001) 498–519. doi:10.1109/18.910572.
- [36] J. Pearl, Probabilistic Reasoning in Intelligent Systems, Kaufmann, San Francisco, 1988.
- [37] J. Winn, C. M. Bishop, Variational Message Passing, *Journal of Machine Learning Research* 6 (2005) 661–694.
- A. Logg, K.-A. Mardal, G. Wells, Automated Solution of Differential Equations by the Finite Element Method: The FEniCS Book, Springer Publishing Company, Incorporated, 2012.
- [39] SGX SensorTech Limited, The MiCS-5524 is a compact MOS sensor, 1084 Rev. 6.
- K. Ihokura, J. J. Watson, The stannic oxide gas sensor : principles and applications, Boca Raton : CRC Press, 1994, includes bibliographical references and index.
- [41] Y. Rubner, C. Tomasi, L. J. Guibas, A Metric for Distributions with Applications to Image Databases, *Computer Vision, 1998. Sixth International Conference on* (1998) 59–66doi:10.1109/ICCV.1998.710701.
- [42] MiCS Application Note 4 Using MiCS Sensors for Alcohol Detection APPLICATION - BREATHALYSER, Tech. Rep. June, SGX sensorTech (2009).

## Author Biography

**Thomas Wiedemann** is a scientist at the Institute of Communications and Navigation, German Aerospace Center, where he is working in the Swarm Exploration Group since 2014.

Further, he is enrolled as a PhD student at the AASS research center, Örebro University.

He obtained a Bachelor and Master degree from the Faculty of Mechanical Engineering at the Technical University of Munich.

His research interests include multi-robot systems, robotic exploration and gas source localization.

**Dmitriy Shutin** received a Master Degree in Computer Science in 2000 from Dnipropetrovsk State University, Ukraine, and the Doctoral degree in Electrical Engineering from Graz University of Technology, Graz, Austria, in 2006.

In 2001-2009 he was with the Signal Processing and Speech Communication Laboratory at Graz University of Technology. In 2009 he joined Department of Electrical Engineering at Princeton University as a Research Associate.

In 2011 he joined the Institute of Communications and Navigation, German Aerospace Center, where he is leading the Swarm Exploration Group.

His research interests include machine learning for signal processing, statistical signal processing, and distributed algorithms.

**Achim J. Lilienthal** is head of the Mobile Robotics and Olfaction Lab at the Center for Applied Autonomous Sensor Systems (AASS), Örebro University, Sweden.

His research interests are mobile robot olfaction, rich 3D perception, robot vision, and autonomous transport robots.

Achim Lilienthal obtained his Ph.D. in computer science from Tübingen University, Germany and his M.Sc. in Physics from the University of Konstanz, Germany.







# Bayesian Gas Source Localization and Exploration with a Multi-Robot System Using Partial Differential Equation Based Modeling

Author1 and Author2

Affiliation 1

Address 1

Author3, Author4 and Author5

Affiliation 2

Address 2

**Abstract**—Model based approaches, such as those that use partial differential equations (PDE), lend themselves to gas distribution mapping and gas source localization. Moreover, they also permit constructing intelligent sampling strategies. However, a realistic mathematical model of gas dispersion is complex and computationally expensive to solve. This is especially the case for inverse problems, where sources are estimated based on concentration measurements. In this paper, we propose a probabilistic model based on a diffusion PDE to approximate the complex behavior of gas dispersion. This model is used (i) to identify the sources, using ideas from Sparse Bayesian Learning, and (ii) to guide a multi-agent robotic system to measurement locations, which assists the source localization. The potential of the approach is shown in experiments, where laminar gas plumes are simulated using an open-source CFD-based filament gas dispersion simulator. The exploration is carried out using multiple real robots implementing the proposed algorithm.

## I. INTRODUCTION

Deploying robotic platforms in hazardous environments for exploration or monitoring has significant practical advantages as it allows avoiding potential threats for human operators. This is particularly important in case of disaster scenarios when a gas concentration has to be mapped, or there is a need to identify unknown gas sources. In this paper we propose a model-based exploration strategy for a multi-robot system that permits detection and localization of unknown gas sources based on agent-mounted sensors. Unfortunately, physical mechanisms causing gas propagation are not trivial, and in case of turbulence can even exhibit non-deterministic and chaotic behavior [3], [9]. Nonetheless, for on-line mapping scenarios a simplified approximation of the physical phenomenon with low computational complexity might be of a great use. To this end in this paper we investigate the capability of a diffusion partial differential equation (PDE) to approximate spatial gas dynamics for the purpose of identifying sources that drive the gas propagation.

The addressed exploration task is closely related to a so called optimal sensor placement problem. Known methods use linear-quadratic control design techniques, which try to optimize the observer performance by adjusting the sensor location [2]. Other popular methods are based on optimal experimental design [8] and probabilistic [4] or Bayesian approaches [7]. In our work we build upon these ideas and propose an exploration strategy that minimizes the uncertainty

of source localization following a criterion similar to an A-optimality [1]. Additionally, similar to [6] we exploit the assumption that the sources causing gas dispersion are sparsely distributed and use sparse Bayesian learning techniques to model this. By using a realistic gas dispersion simulator [5], we demonstrate the effectiveness and performance of the proposed method with a hardware-in-the-loop simulation with five mobile robots in a laboratory environment. The analysis of the experimental data demonstrates the effectiveness of the proposed modeling approach and of the exploration strategy in a multi-agent environment.

## II. GAS DISPERSION SIMULATOR

As previously stated, we validate our proposed algorithms with a state-of-the-art gas dispersion simulator<sup>1</sup>, originally presented in [5]. The simulator is build upon the Robot Operating System (ROS) framework<sup>2</sup>, allowing in this way to simulate gas dispersion, mobile robots and gas sensing technologies in a unified tool. The gas dispersion simulation engine is particle-based. This means that gas concentrations depend on the number of particles, which are affected by diffusion, turbulence, advection, and gravity. Wind information is integrated in the simulation engine as a series of time snapshots that can be computed with an external fluid dynamics tool. In addition, response models for gas sensing devices such as Metal Oxide (MOX) sensors can be integrated in the framework and simulated on board of stationary or mobile platforms. In this work, we neglect the airflow by setting the wind vector field to zero.

## III. MODEL BASED EXPLORATION

### A. Probabilistic model

From a practical perspective, approximating complex gas dynamics with simple models can be of an advantage. Here we use a 2D diffusion model that can be formally described with a linear parabolic partial differential equation (PDE):

$$\frac{\partial f(\mathbf{x}, t)}{\partial t} - \kappa \Delta f(\mathbf{x}, t) = u(\mathbf{x}, t). \quad (1)$$

<sup>1</sup>The simulator is available at the following repository (link removed for the double-blind review)

<sup>2</sup><http://www.ros.org/>

Essentially, (1) models the dynamic behavior of some gas concentration  $f$  at a 2D position  $x$  with respect to time  $t$  given the constant diffusion coefficient  $\kappa$ . The term  $u(x, t)$  on the right hand side represents a spatio-temporal inflow of material; in this work we aim to identify this process.

In order to solve a PDE, numerical approximation methods are often the instrument of choice. To this end we begin with a classical Finite Difference Method [10] which “transforms” (1) into a finite dimensional linear system by appropriately discretizing both space and time:

$$\mathbf{A}[\mathbf{f}[n], \mathbf{f}[n-1], \mathbf{u}[n]]^T = 0; \quad (2)$$

In other words, we divide our region of interest into a finite number of grid cells and consider temporal evolution of concentration values in each cell at discrete time steps  $n$ . Thus, the vector  $\mathbf{f}[n]$  contains the concentration in all grid cells at time stamp  $n$ ; likewise,  $\mathbf{u}[n]$  aggregates the source strength for all grid cells. Both quantities are in general unknown and are estimated numerically using sample observations of the gas concentration at different locations and time instances. Yet we stress that the main interest for us is the estimation of the source distribution  $\mathbf{u}[n]$  as this information guides the dynamic of the whole process.

To facilitate numerical estimation of the PDE parameters we relax (2). This reflects the fact that the real gas dispersion mechanisms are more complex and not always deterministic; thus, we assume that (2) holds only with a certain precision, with deviations from zero being random. This permits us taking a probabilistic approach toward PDE solution by treating all variables as random. This results in a probabilistic formulation, where we can define a conditional probabilistic density function (PDF) for concentrations  $\mathbf{f}[n]$  as follows:

$$p(\mathbf{f}[n]|\mathbf{f}[n-1], \mathbf{u}[n]) \propto e^{-\frac{\tau_s}{2} \| \mathbf{A}[\mathbf{f}[n], \mathbf{f}[n-1], \mathbf{u}[n]]^T \|^2} \quad (3)$$

which is a relaxation of (2) that allows it to deviate from 0 within the precision  $\tau_s$ . In practice the gas concentrations are not observed directly, but are rather measured with a sensor. The actual measurement can be represented as  $\mathbf{y}[n] = \mathbf{M}[n]\mathbf{f}[n] + \boldsymbol{\epsilon}_m$ , where  $\mathbf{M}[n]$  selects grid cells visited by the robots, and  $\boldsymbol{\epsilon}_m$  models a spatially and temporally white measurement noise with precision  $\tau_m$ . The corresponding concentration likelihood can then be expressed as

$$p(\mathbf{y}[n]|\mathbf{f}[n]) \propto e^{-\frac{\tau_m}{2} \| \mathbf{M}[n]\mathbf{f}[n] - \mathbf{y}[n] \|^2}. \quad (4)$$

Now we assume that the sources  $\mathbf{u}[n]$  are sparse in space, i.e., the gas distribution is only driven by a few unknown discrete sources; neither their number nor their location is known. These assumptions can be incorporated using Sparse Bayesian Learning (SBL) techniques (see [11], [12] for more details). SBL assumes a parametric prior  $p(\mathbf{u}[n], \boldsymbol{\gamma}[n])$ , with parameters  $\boldsymbol{\gamma}[n]$  effectively determining if an element in  $\mathbf{u}[n]$  is 0 or not.

Using Bayes theorem, the inference problem reduces to the

calculation of the posterior PDF

$$p(\mathbf{F}, \mathbf{U}, \boldsymbol{\Gamma} | \mathbf{Y}) \propto \prod_{n=1}^N p(\mathbf{y}[n]|\mathbf{f}[n])p(\mathbf{f}[n]|\mathbf{f}[n-1], \mathbf{u})p(\mathbf{u}[n], \boldsymbol{\gamma}[n]) \quad (5)$$

where, with some abuse of notation, we use the capital letters to define the aggregation of the corresponding variable over the whole observation time, i.e.,  $\mathbf{F} = [\mathbf{f}[0], \dots, \mathbf{f}[N-1]]$ . Effectively, (5) defines the most likely gas concentration  $\mathbf{F}$  and source locations  $\mathbf{U}$  given all available measurements. Note that SBL not only “sparsifies” vector  $\mathbf{u}[n]$ , but also regularizes the solution. This is important as in early stages, when the number of measurement is smaller than the number of unknowns –  $\mathbf{f}[n]$ ,  $\mathbf{u}[n]$  and  $\boldsymbol{\gamma}[n]$  – the resulting optimization problem is ill-posed.

### B. Exploration strategy

While movements of the agents can be arbitrary, it is advantageous when their trajectories are selected to facilitate estimation of the sources  $\mathbf{u}[n]$ . This is the objective of the exploration strategy discussed below. Note that the probabilistic approach permits us to quantify the uncertainty of the source strength in each grid cell. In our approach we take into account the individual marginal PDF for each element of  $\mathbf{u}[n]$ . Specifically, that a high variance of the estimated source marginal PDFs implies a high uncertainty. This quantity can be used to rate all cells in the region of interest, and cells with highest uncertainties are provided to the multi-agent system as proposals for new measurement locations. Each robot selects a cell based on the uncertainty value and additionally weighted by the distance to it. In other words, the robots not only prefer cells with high uncertainty but also cells which are close to their current positions. When a target is reached, a measurement is taken, which maximally reduces the uncertainty of the corresponding grid cells. This can be shown to be equivalent to a so called A-optimality criteria. Then the model is updated by (i) adapting the measurement vector  $\mathbf{y}[n]$  and matrix  $\mathbf{M}[n]$ , and (ii) performing inference of the current states  $\mathbf{f}[n]$  and sources  $\mathbf{u}[n]$ . After that the whole scheme is repeated. By successively improving each individual cell, this exploration strategy minimizes the overall uncertainty of the source distribution. Note that practically some collision avoidance mechanism is needed. To this end in the discussed experiments a simple scheme to avoid collisions is realized on a lower control layer.

## IV. RESULTS

For evaluation purposes, we used the gas dispersion simulator to generate a dynamic gas distribution driven by one source in an area of 20m times 60m. This area is virtually scaled down by factor 10 to fit into our laboratory environment. Whenever a robot is triggered to collect a measurement, the simulated gas concentration at the robots position is used as a synthetic measurement for the exploration algorithm. The diffusion coefficient  $\kappa$  of the PDE model is estimated in a

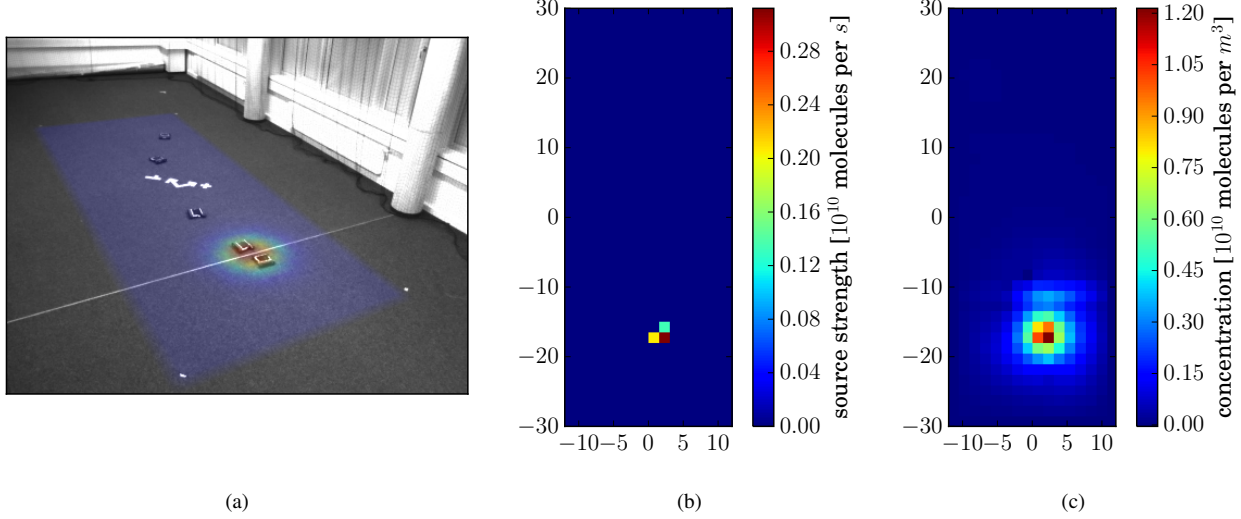


Fig. 1. Snapshot of the exploration procedure at a certain time stamp (marked in Fig 2): In (a) a picture of the multi-robot system is shown overlayed by the simulated gas distribution. Plot (b) displays the estimated source distribution and (c) the estimated gas concentration.

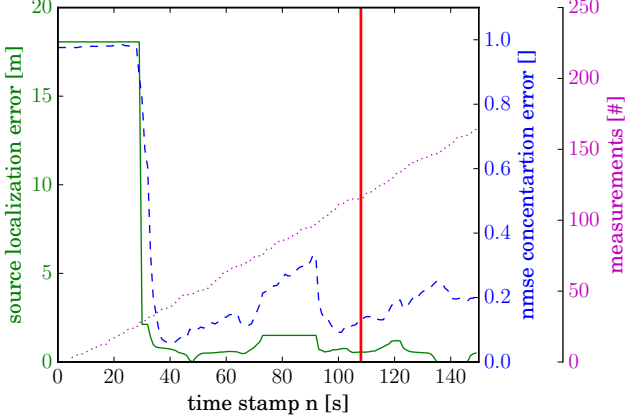


Fig. 2. Performance of the exploration: The source localization error is calculated by comparing the center of mass of the estimated source distribution with the actual position of the source used in the simulation. The concentration estimate is assessed by the normalized mean square error (nmse) with respect to the concentration given by the simulator.

pre-processing step to best approximate the gas dispersion. Fig. 1 visualizes the result of the exploration at a certain time step, whereas Fig. 2 depicts the performance of the estimates over time. Although the difference between the simulated gas concentration and the estimated concentration based on the simplified model is rather high due to the oversimplifying diffusion approximation, the estimated source strength distribution is quite accurate and the robots are able to localize the source in a reasonable time frame with good accuracy.

## V. CONCLUSION

The paper showed that it is possible, to some extend, to approximate a complex gas dispersion phenomenon by a simplified model. We exploited this model to design an exploration strategy for a multi-robot system that facilitates

the localization of sources driving the phenomenon. In future work, we will extend the approach to better cope with advection mechanisms by introducing a convection term into the PDE.

## REFERENCES

- [1] A. Alexanderian, N. Petra, G. Stadler, and O. Ghattas, “A-optimal design of experiments for infinite-dimensional Bayesian linear inverse problems with regularized 10-sparsification,” *SIAM Journal on Scientific Computing*, vol. 36, no. 5, p. 27, 2013.
- [2] M. Demetriou, “Numerical investigation on optimal actuator/sensor location of parabolic PDEs,” *Proceedings of the 1999 American Control Conference*, vol. 3, no. June, pp. 1722–1726, 1999.
- [3] V. Hernandez, A. J. Lilienthal, P. P. Neumann and M. Trincavelli, “Mobile robots for localizing gas emission sources on landfill sites: is bio-inspiration the way to go?,” *Front. in Neuroeng.*, 4: 0, 2012.
- [4] J. Kaipio and E. Somersalo, *Statistical and Computational Inverse Problems*, 1st ed. Springer-Verlag New York, 2005.
- [5] A. Khalil, S. Pashami, E. Schaffernicht, A. J. Lilienthal and V. Hernandez, “Bringing Artificial Olfaction and Mobile Robotics Closer Together - An integrated 3D Gas Dispersion Simulation in ROS,” Proc. of the 16th Intl. Symposium on Olfaction and E-Noses (ISOEN), 2015.
- [6] K. Kunisch, K. Pieper, and B. Vexler, “Measure Valued Directional Sparsity for Parabolic Optimal Control Problems,” *SIAM Journal on Control and Optimization*, vol. 52, no. 5, pp. 3078–3108, jan 2014.
- [7] D. J. C. MacKay, “Information-Based Objective Functions for Active Data Selection,” *Neural Computation*, vol. 4, no. 4, pp. 590–604, 1992.
- [8] F. Pukelsheim, *Optimal Design of Experiments*. John Wiley & Sons, Inc., 1993.
- [9] Roberts, P., and Webster, “Turbulent Diffusion. Environmental Fluid Mechanics Theories and Application”, Reston, VA: ASCE Press, 2002.
- [10] Strikwerda, J.C.: *Finite Difference Schemes and Partial Differential Equations*, 2 edn. Society for Industrial and Applied Mathematics, Philadelphia (2004)
- [11] M. E. Tipping, “Sparse Bayesian Learning and the Relevance Vector Machine,” *Journal of Machine Learning Research*, 2001.
- [12] D. P. Wipf and B. D. Rao, “Sparse Bayesian learning for basis selection,” *Signal Processing, IEEE Transactions on*, vol. 52, no. 8, pp. 2153–2164, 2004.